



A Comprehensive Analysis of AOD and its Species from Reanalysis Data over the Middle East and North Africa Regions: Evaluation of Model Performance Using Machine Learning Techniques

Samuel Abraham Berhane^{1,2} · Pelati Althaif³ · Kanike Raghavendra Kumar^{1,3} · Lingbing Bu¹ · Muxi Yao⁴

Received: 12 August 2024 / Revised: 18 October 2024 / Accepted: 23 October 2024

© King Abdulaziz University and Springer Nature Switzerland AG 2024

Abstract

The present study examines the spatiotemporal changes in aerosol optical depth (AOD) and five aerosol species over the Middle East and North Africa (MENA) regions and incorporates an advanced Machine Learning model to predict AOD. The study utilizes reanalysis data from the Modern-Era Retrospective Analysis for Research and Applications, version 2 (MERRA-2), and the Copernicus Atmosphere Monitoring Service Reanalysis (CAMSRA), in conjunction with the MODIS spanning from 2003 to 2020. Seasonal-averaged AOD_{550} showed the dominance of aerosols in the summer and spring seasons, primarily driven by dust and black carbon, with dust being the most significant contributor due to frequent storms and desert conditions. Other contributors such as sea salt, sulfate, and organic carbon also play crucial roles, underscoring the complex interplay between natural and anthropogenic aerosols. The validation results revealed a high coefficient of determination (R^2) for AOD ranging from 0.76 to 0.96 across these datasets. This demonstrates strong predictive accuracy with the XGBoost model, which shows a robust correlation between predicted and actual AOD values with minimal error and no significant bias. The AI/ML model analysis further elucidates the contributions of individual aerosol species to AOD predictions, revealing that dust and black carbon consistently enhance AOD. This study reveals that AOD fluctuations in the MENA region are driven by meteorological factors and drought-induced dust emissions. Ultimately, long-term reliable atmospheric composition reanalysis data can supplement ground-based or remote sensing observations in air quality research, emphasizing the need for continuous assessment of aerosols to inform policies aimed at reducing air pollution and mitigating climate change impacts.

Keywords Aerosol Optical Depth · CAMSRA · Machine Learning Model · MERRA-2 · Middle East · North Africa

Kanike Raghavendra Kumar
kanike.kumar@gmail.com

Lingbing Bu
lingbingbu@nuist.edu.cn

¹ Collaborative Innovation Center on Forecast and Evaluation of Meteorological Disasters, Key Laboratory for Aerosol-Cloud-Precipitation of China Meteorological Administration, Key Laboratory of Meteorological Disasters, Ministry of Education, Nanjing University of Information Science and Technology, Nanjing 210044, China

² Eritrean Meteorological Services Department, Asmara International Airport Authority, Ministry of Transport and Communications, Asmara 5846, Eritrea

³ Department of Engineering Physics, College of Engineering, Koneru Lakshmaiah Education Foundation (KLEF), Vaddeswaram, Guntur 522302, Andhra Pradesh, India

⁴ Department of Hydrology and Atmospheric Sciences, The University of Arizona, Tucson, AZ 85721, USA

1 Introduction

Atmospheric aerosols are tiny particles that exist in a solid or liquid state and are suspended in the atmosphere. They interact with the atmosphere by scattering or absorbing solar radiation (known as the direct effect) and by altering cloud particles (referred to as the indirect effect), which can lead to reduced precipitation (Charlson et al. 1992; Ramanathan et al. 2001). Aerosols significantly influence climate while introducing considerable uncertainty into the Earth's radiation budget (IPCC 2021; Rosenfeld et al. 2014). They have important impacts on climate change at both regional and global scales, as well as on air quality, which poses risks to the environment and public health. In this regard, climate researchers, atmospheric scientists, and public health professionals acknowledge the importance of understanding

the spatiotemporal variations, as well as the physical, chemical, radiative, and dynamical characteristics of aerosols at local, regional, and global levels. One of the key properties of aerosols that are commonly analyzed is aerosol optical depth (AOD), which is defined as the integral of the extinction coefficient along a vertical column with a unit cross-section (Althaaf et al. 2024; Boiyo et al. 2017).

The Middle East and North Africa (MENA) region plays a critical role as one of the world's largest sources of aeolian dust, with approximately 500 to 3,000 billion tons emitted into the atmosphere annually (Shaheen et al. 2020). These dust emissions, primarily originating from the vast deserts and semi-arid areas in the region, significantly impact environmental, climatic, and health-related processes (Yousefi et al. 2023; Berhane et al. 2024). The MENA region is especially vulnerable to the complex interplay between natural and anthropogenic aerosols, which contribute to the region's dynamic climate. Dust particles influence air temperature, cloud condensation nuclei (CCN), and consequently, precipitation patterns (Yu et al. 2016; Ramachandran et al. 2012). Despite considerable research into the direct radiative effects of dust, which include absorption and scattering of solar and thermal radiation, the indirect effects on cloud microphysics and rainfall remain an area of high uncertainty (Francis et al. 2021).

The MENA region is recognized as a climate change hotspot, experiencing heightened dust storm activity and variability in AOD (Almazroui 2022; Khamala et al. 2024; Berhane et al. 2024). The region is characterized by dust storms that are primarily seasonal, occurring during spring and early summer over the Iraqi, Saudi Arabian, and Libyan-Egyptian deserts, and play a critical role in aerosol transport, affecting local weather and global precipitation patterns (Andreae and Rosenfeld 2008; Li et al. 2016). While satellite-based remote sensing techniques, such as those employed by the SeaWiFS and MODIS satellites, have shown increasing AOD trends in the region during the early 2000s (Hsu et al. 2012). Recent studies suggest a reversal in this trend, indicating a more complex temporal and spatial aerosol distribution (Shaheen et al. 2022, 2024). In addition to natural dust emissions, the MENA region is experiencing increasing contributions from anthropogenic sources due to urbanization and industrialization, particularly in major cities where particulate matter (PM) levels are elevated (Shahid et al. 2021; Berhane et al. 2024). The combination of natural dust and anthropogenic aerosols creates intricate aerosol mixtures that influence both regional and global climate patterns (Parajuli et al. 2020).

The MENA regions are among the significant areas of the world where the prominent natural sources of aerosols are desert dust (Knippertz and Todd 2012; Ryder et al. 2013; Goudie 2014; Tindan et al. 2023; Kuttippurath and Raj

2021). Both anthropogenic and natural aerosols tend to contribute to the fluctuation of seasonal climate characteristics in this region (Berhane and Bu 2021; Berhane et al. 2024). The Sahara Desert forms due to its location in the subtropical high-pressure belt, leading to arid conditions and limited vegetation (Wang et al. 2015), and wind erosion shapes its dunes and rock structures. The region's topography results from tectonic activity, climate, and erosion (Migoñ et al. 2017). Notably, the Saharan Air Layer (SAL) carries desert dust westward across the Atlantic Ocean, affecting air quality, climate, weather, and ecosystems (Prospero et al. 2021). The major city centers in the Middle East have high PM levels due to urbanization and industrialization (Shahid et al. 2021).

Although numerous studies have been conducted in the MENA region, a considerable gap remains in our understanding of the specific characteristics of aerosols, particularly regarding their type, behavior, spatial distribution and trends across different seasons. This study seeks to fill that gap by offering a comprehensive analysis of aerosol dynamics in the MENA region, thereby enhancing our understanding of their effects on local meteorological conditions. Furthermore, the interplay between dust storms and anthropogenic pollutants creates complex aerosol mixtures that affect both local and regional climates (Parajuli et al. 2020; Shahid et al. 2021). Consequently, this aerosol transport alters the cloud and precipitation patterns in the region (Li et al. 2016; Gunthe et al. 2021; Shaheen et al. 2024). Several studies, including ground-based instruments like the Aerosol Robotic Network (AERONET), are employed to measure AOD in the North and East African regions (Assiri 2024; Kinne et al. 2003; Boiyo et al. 2018; Xu et al. 2020; Sangura et al. 2024). Satellite-based remote sensing techniques can complement ground-based station datasets, particularly in areas unsuitable for ground instruments and over oceanic regions. A study by, also depicted the future dust concentration in the MENA region under global warming and stratospheric aerosol intervention scenarios. Also, the effects of bioaerosols on human health and their long-range transportation from North Africa are reported by Karami et al. (2020).

The present study utilizes the eXtreme Gradient Boosting (XGBoost) machine learning model to analyze and predict aerosol dynamics over the MENA region from 2003 to 2020, focusing on AOD and its driving environmental factors. The XGBoost model can handle large datasets and complex relationships making it ideal for studying spatiotemporal aerosol variations in this dust-prone region. The novelty of this research lies in the application of feature importance analysis to identify key factors influencing aerosol levels, SHAP (SHapley Additive exPlanations) value plots for model interpretability, and comparisons between actual and

predicted AOD values to validate model accuracy. This AI/ML approach of the XGBoost model provides new insights into aerosol behavior, enhancing the understanding of environmental drivers in the MENA region and contributing to improved forecasting and climate policy decisions.

The present study evaluates a comprehensive analysis of the spatial distributions of AOD and aerosol species in the MENA region from 2003 to 2020. This study utilizes the global satellite and reanalysis datasets from the Modern-Era Retrospective Analysis for Research and Applications, Version 2 (MERRA-2) and the Copernicus Atmosphere Monitoring Service Reanalysis (CAMSRA) datasets along with the Moderate-resolution Imaging Spectroradiometer (MODIS). In addition to this, the integration of Machine Learning (ML) models, such as XGBoost incorporated to enhance the prediction and analysis of AOD, providing deeper insights into aerosol behaviour and its influencing factors across the MENA regions. The entire study area, the MENA region, is divided into five regions: Sahel-Sahara Desert (SSD), East Africa (EA), North Africa (NA), Middle East (EA), and Central and West Africa (CWA) (see Fig. 1). The investigation covers all four seasons: winter (from December to February; DJF), spring (from March to May; MAM), summer (from June to August; JJA), and autumn

(from September to November; SON). The subsequent section explores the description, data retrieval procedures, and accuracies of different satellite and reanalysis data products. Section 3 investigates the detailed graphical analysis of data followed by a discussion of the obtained results. The research paper provides concluding remarks and its summary in the final section.

2 Satellite Data

2.1 The CAMSRA Datasets

The European Centre for Medium-Range Weather Forecasts (ECMWF) offers a range of reanalysis data products, continually improving model and data configurations, as well as updating emissions and satellite retrievals. Among these products are ERA-5, MACRA, CAMS reanalysis (CAMSRA), and CAMS interim reanalysis (CIRA) (Inness et al. 2019). The CAMSRA, a recent ECMWF reanalysis dataset, focuses on atmospheric composition, providing 3-dimensional time-consistent data for atmospheric composition, including aerosols, chemical species, and greenhouse gases (GHGs). This study utilizes CAMSRA data spanning from

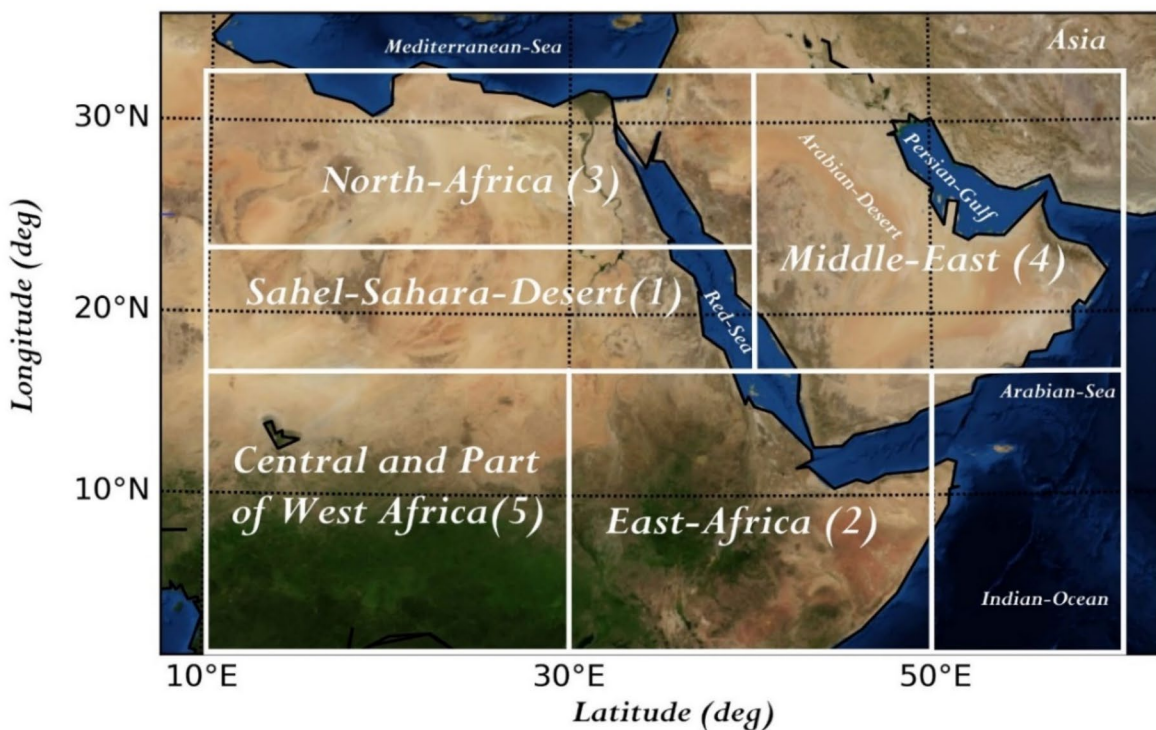


Fig. 1 Map of the study area, highlighting distinct regions: the Sahel-Sahara Desert (SSD), East Africa (EA), North Africa (NA), Middle East (ME), and Central and a portion of West Africa (CWA). Numbers from one (1) to five (5), respectively denote these areas

2003 to 2020, featuring a 0.75° spatial resolution (Flemming et al. 2017; Inness et al. 2019). CAMSRA demonstrates a lower bias compared to other products produced using 4DVar data assimilation in the ECMWF Integrated Forecasting System (IFS) Cycle 42r1. CAMSRA incorporates 60 hybrid sigma/pressure levels vertically, with the highest level at 0.1 hPa. The datasets are available on these levels and interpolated to 25 pressure levels in “surface or single-level”, 10 potential temperature levels, and 1 potential vorticity level (Inness et al. 2019). CAMSRA ensures temporal consistency by being developed from a single version of the model and assimilation system, specifically IFS (CB05), minimizing potential changes due to emissions or assimilated satellite products (Flemming et al. 2017).

Table 1 The details of different datasets retrieved from satellites used in this study

| Satellite | Variable/Product name and its wavelength | Spatial resolution | Temporal resolution | Time Range |
|-----------|---|------------------------------------|---------------------|------------|
| MOD08_M3 | AOD_550_Dark_Tar-get_Deep_Blue_Combined_Mean | $1^{\circ} \times 1^{\circ}$ | Monthly | 2003–2020 |
| MYD08_M3 | AOD_550_Dark_Tar-get_Deep_Blue_Combined_Mean | $1^{\circ} \times 1^{\circ}$ | Monthly | 2003–2020 |
| CAMSRA | Total Aerosol Optical Depth at 550 nm Black Carbon Aerosol Optical Depth at 550 nm Dust Aerosol Optical Depth at 550 nm Organic Matter Aerosol Optical Depth at 550 nm Sea Salt Aerosol Optical Depth at 550 nm Sulfate Aerosol Aerosol Optical Depth at 550 nm | $0.75^{\circ} \times 0.75^{\circ}$ | Monthly | 2003–2020 |
| MERRA-2 | Total Aerosol Extinction AOT (550 nm) Dust Extinction AOT (550 nm) Organic Carbon Extinction AOT (550 nm) Black Carbon Extinction AOT (550 nm) Sea Salt Extinction AOT (550 nm) SO_4 Extinction AOT (550 nm) | $0.5^{\circ} \times 0.625^{\circ}$ | Monthly | 2003–2020 |

Throughout the study period, CAMSRA assimilates total AOD retrievals at 550 nm from MODIS on Aqua and Terra satellites (Factorization 2019; Liu et al. 2021; Ali and Assiri 2019). It also incorporates AOD retrievals from the Advanced Along-Track Scanning Radiometer (AATSR) on Envisat from 2003 to 2012 (Sogacheva et al. 2017). Both MODIS and AATSR retrievals undergo a variation bias correction scheme to ensure consistency and temporal stability when using different datasets (Inness et al. 2019; Liu et al. 2021). CAMSRA AOD products encompass the AOD of five aerosol species: sea salt, dust, organic carbon (OC), black carbon (BC), and sulfate. Each aerosol species is computed using the standard Lorentz–Mie algorithm, assuming external mixing, and is corrected based on their relative contributions to total aerosol (Liu et al. 2021). These five AOD variables have an 80 km ($\sim 0.75^{\circ}$) spatial resolution (see Table 1).

2.2 The MERRA-2 Reanalysis Data

NASA’s MERRA-2 is an advanced atmospheric reanalysis crafted by NASA’s Global Modeling and Assimilation Office (GMAO) (Gelaro et al. 2017). Building on MERRA, it integrates new observation types and improves the Goddard Earth Observing System (GEOS) model, making it versatile for various weather and climate applications (McCarty et al. 2016). It also benefits from advancements in the GEOS model and Grid-point Statistical Interpolation (GSI) analysis technique, advancing GMAO’s Earth System reanalysis vision (Nielsen et al. 2017; Zhang et al. 2020; Althaf et al. 2024; Sanatan et al. 2024). MERRA-2’s notable feature is its ability to assimilate long-term records of atmospheric aerosols, making it the first global reanalysis to account for aerosol impacts on climate processes, demonstrating GMAO’s commitment to ongoing climate analysis (Weir et al. 2021; Masoud 2023). In the GEOS-5 system, MERRA-2 combines aerosol and meteorological observations, carefully screening clouds for consistency (da Silva et al. 2013). Since 2002, it has integrated bias-corrected AOD data from MODIS collection 5, Level 2 radiances from Terra and Aqua satellites, also assimilating AOD data from MISR over bright surfaces and surface-based AERONET AOD observations at 550 nm (Liu et al. 2021). MERRA-2 provides AOD data for five aerosol species, closely aligning with CAMSRA, and employs an external mixing assumption (Ou et al. 2022). MERRA-2 offers the highest spatial resolution of $0.5^{\circ} \times 0.625^{\circ}$ (Table 1) among the three datasets.

2.3 The MODIS Sensor

The MODIS instrument operates on both the Terra and Aqua spacecraft, with a viewing swath width of 2,330 km, covering the entire Earth's surface every one to two days (Remer et al. 2005 and references therein). At the equator, Terra overpasses at 10:30 h LT (Local Time), while Aqua overpasses at 13:30 h LT, crossing from north to south (<https://modis.gsfc.nasa.gov/>). It measures 36 spectral bands from 0.405 to 14.385 μm and acquires data at three spatial resolutions: 250 m, 500 m, and 1,000 m. Two algorithms track AOD from satellite remote sensing observations: the Dark Target (DT) algorithm for aerosol data over ocean, vegetation, and surfaces with lower reflection, and the Deep Blue (DB) algorithm for surfaces with higher reflectivity like deserts (Levy et al. 2010). The combination of MODIS DT and DB AOD data aligns well with ground-based observations (Boiyo et al. 2017; Gupta et al. 2020; Huang et al. 2020). Several studies have evaluated the impact of assimilating MODIS AOD data using different algorithms and found that the combined DT and DB AOD data match ground truth equally well with existing MODIS products and, in some cases, perform better (Choi et al. 2020; Huang et al. 2023). This study uses the level-3 monthly mean of Combined DT and DB AOD at 0.55 microns (MOD08_D3_v6, Version C6.1) for land and ocean. The monthly mean MODIS AOD₅₅₀ data cover the period from January 2003 to December 2020, at a spatial resolution of 1° x 1° (details in Table 1).

2.4 XGBoost Technique

The study also effectively employs the eXtreme Gradient Boosting (XGBoost) model framework for time-series prediction of AOD and its associated aerosol species in the MENA region from 2003 to 2023. XGBoost, known for its superior predictive capabilities and efficiency, is selected after demonstrating its outperforming statistical models in predicting aerosol concentrations (Gui et al. 2020). The study utilizes key statistical metrics- Pearson's correlation, mean bias error (MBE), and root-mean-square error (RMSE) to evaluate model performance, alongside K-fold cross-validation (CV) for robust validation. Additionally, feature importance is assessed through F-score values and SHAP analysis to elucidate the influence of various aerosol species on AOD predictions. Notably, XGBoost, an artificial intelligence (AI)-driven machine learning (ML) model, was implemented for the first time in the MENA region, highlighting innovative applications in air quality monitoring and pollution research.

3 Results and Discussion

3.1 Validation Results Between AERONET and MODIS

A comparative analysis of AOD₅₅₀ derived from AERONET and MODIS datasets was conducted across five designated geographic stations, namely KAUST-Campus (22.305°N, 39.103°E), Kuwait University (29.325°N, 47.971°E), Medenine-IRA (33.5°N, 10.643°E), ICIPE-Mbita (0.432°S, 34.206°E), and EL_Farafra (27.058°N, 27.990°E). ICIPE-Mbita was chosen as a reference frame due to its alignment with the study area's requirements, notwithstanding a minor deviation of 0.432° to the south. The scatter correlation analysis presented in Fig. 2 reveals a coefficient of determination (R^2) exceeding 0.7 for all investigated stations. This outcome underscores a substantial agreement between AERONET and MODIS AOD measurements. The consistently high R^2 values obtained across the study sites emphasize the reliability of MODIS as a dependable source for AOD information within these specific geographic regions. This outcome emphasizes the capability of MODIS to capture the variations in AOD across diverse geographic landscapes in the MENA region.

In examining the specific AOD₅₅₀ values across the five stations, it is found that the highest R^2 values were recorded at KAUST-Campus and Kuwait University. This suggests that these locations might be more influenced by anthropogenic activities, which are typically better captured by satellite observations. Conversely, the ICIPE-Mbita station, located near the equator, exhibited slightly lower R^2 values. This is attributed to the complexities introduced by local meteorological conditions and varying aerosol sources, including biomass burning and natural dust events. The consistently high R^2 values across all study sites not only underscore the reliability of MODIS as a dependable source for AOD information but also highlight the importance of cross-validation with ground-based measurements like AERONET. This validation process is critical for enhancing the accuracy of satellite-derived AOD data, particularly in regions characterized by diverse aerosol sources, and complex atmospheric and meteorological conditions. Furthermore, the analysis of the scatter plots indicates that while the overall trend of AOD is well-captured by MODIS, there may be systematic biases present at certain locations. For instance, some sites may show a tendency for MODIS to underestimate or overestimate AOD values during specific seasons, particularly during dust storms or periods of high pollution. However, future investigations should focus on identifying these biases and understanding the underlying factors contributing to discrepancies between satellite and ground-based measurements. This will facilitate more

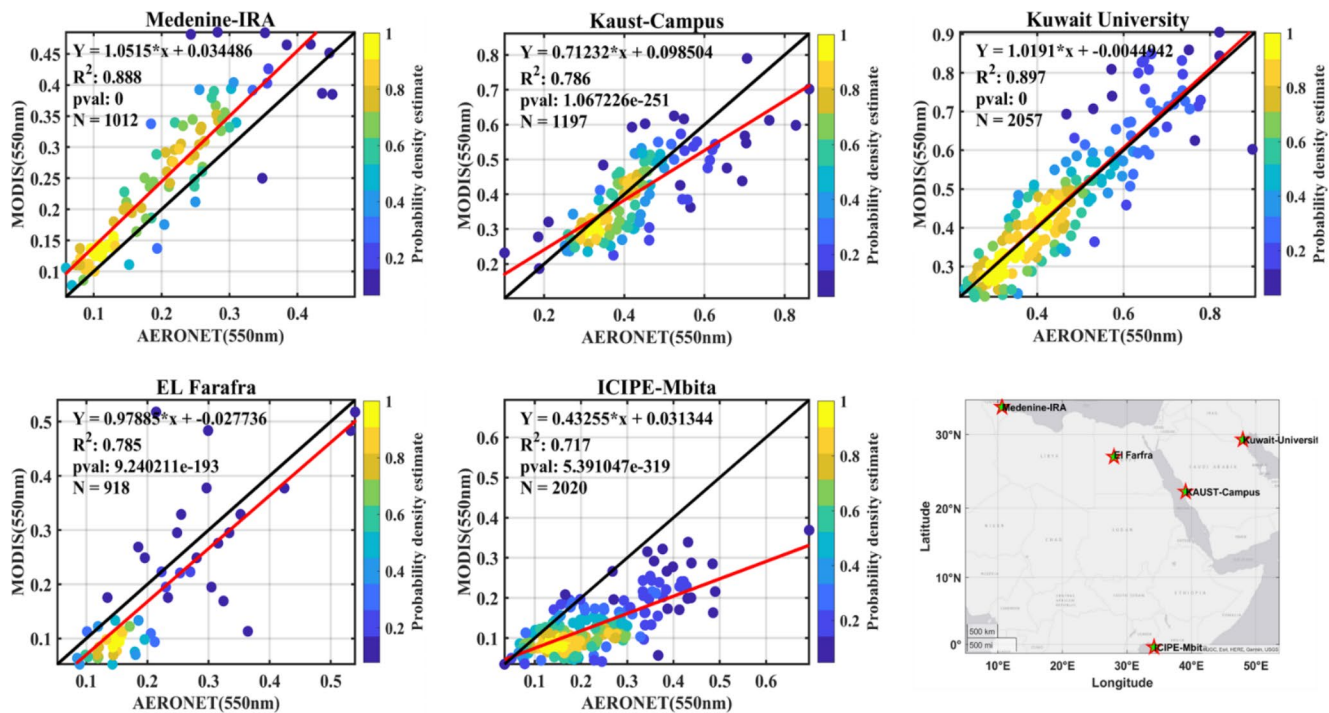


Fig. 2 Validation of AOD₅₅₀ between MODIS versus AERONET in KAUST-Campus (22.305°N, 39.103°E), Kuwait University (29.325°N, 47.971°E), Medenine-IRA (33.5°N, 10.643°E), ICIPE-

Mbita (0.432°S, 34.206°E), and EL_Farafra (27.058°N, 27.990°E). The location of each of the stations is shown in the bottom right panel

refined calibration of satellite data, ultimately improving the assessment of aerosol impacts on climate and air quality within the MENA region.

3.2 Spatiotemporal Variations in AOD

The analysis of seasonal-mean AOD patterns, as ascertained from multiple sources including MODIS, CAMSRA, and MERRA-2 reanalysis data, within the study area is depicted in Fig. 3. The discernible concentration of increased pollution levels, characterized by increased AOD, is particularly conspicuous within regions encompassing the Sahara Sahel Desert (SSD), the Middle East (ME), and Central-West Africa (CWA). The SSD region, known as a potent source of mineral dust due to its vast arid expanse, facilitates the entrainment of particulate matter into the atmosphere via., wind-driven processes (Wang et al. 2015; Menut et al. 2019; Berhane et al. 2024). Similarly, the Middle East and the Central-West African regions are influenced by local geological and meteorological conditions that contribute to aerosol generation and transport. These regions often experience arid climates and periodic dust storms, enhancing the propensity for aerosol suspension (Knippertz et al. 2012; Vandenbussche and De Mazière 2017; Aklesso et al. 2018; Berhane et al. 2024).

Table 2 presents the mean values of AOD derived from the MODIS, MERRA-2, and CAMSRA, across distinct

regions. The evaluation of the mean values of AOD in the Middle East (ME) region stands out, indicating the highest aerosol loading across the three datasets. The high AOD values are notable over the Middle East during the summer months possibly due to a combination of atmospheric and meteorological factors. The region experiences frequent and intense dust storms, driven by atmospheric instability and strong winds which are the seasonal characteristics of the domain. Hot and dry conditions prevalent in summer favor the suspension of dust particles in the atmosphere (Klingmüller et al. 2016; Li et al. 2021; Kunchala et al. 2024). The arid summer climate also enhances dust emissions from the soil. Additionally, longer daylight hours can increase photochemical reactions, potentially forming secondary aerosols. While natural sources dominate, human activities such as increased energy consumption for cooling may also play a role. These combined factors create a distinct seasonal pattern, with AOD values typically peaking from June to September in the Middle East region, as confirmed by observational data and climate models (Berhane et al. 2024).

In the SSD region, total AOD values are higher than those of the CWA regions following the MERRA-2 dataset. Consequently, the CWA region exhibits a high AOD over the SSD region. The North Africa (NA) region demonstrates lower mean AOD values than the ME, CWA, and SSD regions, respectively. However, the lowest AOD was

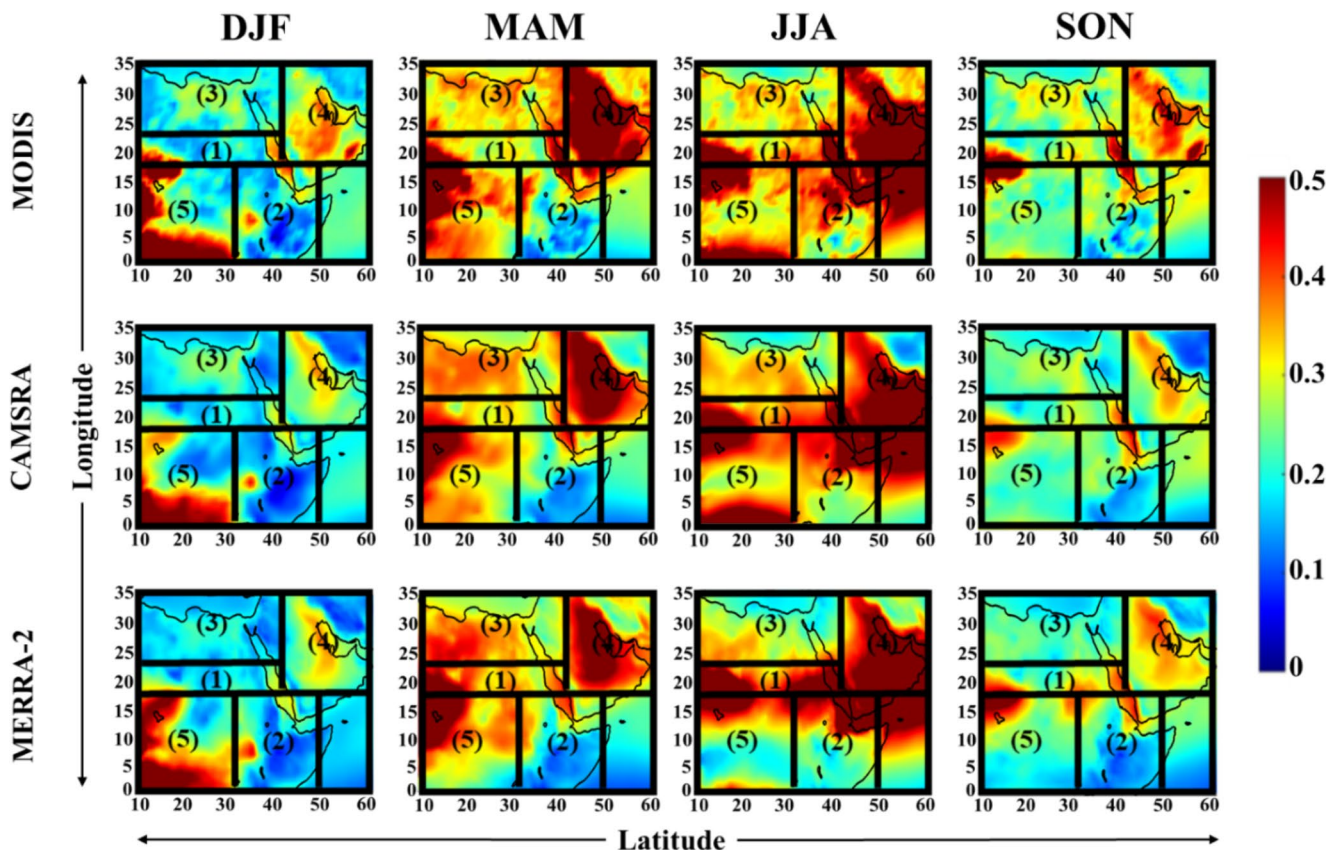


Fig. 3 Spatial distributions of seasonal-mean AOD over the Study area during 2003–2020. Numbers from one (1) to five (5) respectively denote the areas given in Fig. 1

noticed in the East Africa (EA) region among the studied areas. The three datasets showed similar trends in their amplitudes of measurement although AOD from MODIS holds the highest magnitude of AOD measurements except in the SSD region. However, the MERRA-2 AOD values showed higher values than the MODIS dataset. Both the MERRA-2 and CAMSRA datasets showed closer proximity with considerable differences in AOD with similar trends in all regions, except, in the SSD region. The AOD values of CAMSRA and MERRA-2 reanalysis datasets deviate more in the SSD and the Arabian Desert regions due to significant differences in the AOD estimates between the two datasets. Research indicates that the AOD estimates from MERRA-2 were found to be underestimated significantly compared to CAMSRA in these specific desert regions (Shaheen et al. 2020). This discrepancy could be attributed to various factors such as differences in data assimilation methods, model configurations, and input parameters used in generating reanalysis datasets, leading to contrasting estimations of aerosol optical properties in these arid regions (Sangura et al. 2024; Islam et al. 2019).

The geographically localized areas exhibiting substantially elevated AOD values (>0.5) are attributed to a confluence of factors that perpetuate the accumulation of aerosols.

Geographical proximity to deserts, like the Sahara and the Arabian Deserts, offers an ample supply of dust particles that can become airborne through mechanical agitation and lofted by atmospheric updrafts. Furthermore, the proximity to tropical latitudes renders these regions more susceptible to atmospheric instability and convergence of air masses, thereby facilitating the transport and accumulation of aerosols (Huneeus et al. 2011; Rosenfeld et al. 2014). Seasonally, the observed elevated AOD values align and are associated with meteorological and climatic dynamics. The summer and spring seasons emerge as periods of pronounced aerosol loading, a consequence of favorable conditions for aerosol mobilization agreement with the earlier research (Althaaf et al. 2024; Shaheen et al. 2020, 2024; Berhane et al. 2024).

During summer and spring, increased temperatures and intensified surface winds enhance dust mobilization and transport. The resulting elevated AOD values are indicative of a substantial presence of aerosols in the atmospheric column (Aklesso et al. 2018; Laruelle et al. 2014; Ridley et al. 2014; Deflorio et al. 2014; Boiyo et al. 2016, 2018). This phenomenon resonates with the studies on dust storms and their prevalence during warmer seasons. Intriguingly, the winter season also reveals notable aerosol concentrations, albeit concentrated within the CWA region. The comparison

Table 2 Mean AOD₅₅₀ patterns over distinct regions (SSD, EA, NA, ME, and CWA) from 2003 to 2020, were analyzed using the MODIS (MOD), MERRA-2 (MER), and CAMSRA (CAM). The mean AOD and corresponding standard deviation (SD) values are presented to easily evaluate the aerosol loading over each distinct region. The maximum AOD values according to each region are denoted as bold

| Year | SSD | | | EA | | | NA | | | ME | | | CWA | | |
|------|-------------|-------------|-------------|-------------|-------------|-------------|-------------|-------------|-------------|-------------|-------------|-------------|-------------|-------------|-------------|
| | MOD | MER | CAM |
| 2003 | 0.35 | 0.36 | 0.31 | 0.26 | 0.23 | 0.30 | 0.26 | 0.28 | 0.41 | 0.36 | 0.33 | 0.38 | 0.33 | 0.34 | 0.34 |
| 2004 | 0.33 | 0.34 | 0.3 | 0.24 | 0.23 | 0.29 | 0.26 | 0.28 | 0.35 | 0.33 | 0.29 | 0.40 | 0.34 | 0.37 | 0.35 |
| 2005 | 0.34 | 0.37 | 0.31 | 0.25 | 0.23 | 0.29 | 0.27 | 0.28 | 0.37 | 0.34 | 0.30 | 0.38 | 0.34 | 0.35 | 0.35 |
| 2006 | 0.35 | 0.36 | 0.32 | 0.27 | 0.23 | 0.24 | 0.30 | 0.27 | 0.28 | 0.41 | 0.36 | 0.33 | 0.37 | 0.32 | 0.34 |
| 2007 | 0.35 | 0.37 | 0.32 | 0.27 | 0.24 | 0.24 | 0.30 | 0.27 | 0.28 | 0.41 | 0.37 | 0.33 | 0.37 | 0.33 | 0.33 |
| 2008 | 0.34 | 0.37 | 0.31 | 0.28 | 0.26 | 0.25 | 0.29 | 0.28 | 0.47 | 0.41 | 0.37 | 0.36 | 0.33 | 0.32 | 0.32 |
| 2009 | 0.34 | 0.36 | 0.3 | 0.27 | 0.25 | 0.24 | 0.29 | 0.26 | 0.27 | 0.47 | 0.40 | 0.37 | 0.37 | 0.33 | 0.33 |
| 2010 | 0.37 | 0.40 | 0.33 | 0.28 | 0.26 | 0.27 | 0.31 | 0.30 | 0.29 | 0.40 | 0.38 | 0.34 | 0.38 | 0.33 | 0.35 |
| 2011 | 0.36 | 0.37 | 0.31 | 0.32 | 0.28 | 0.29 | 0.29 | 0.27 | 0.27 | 0.46 | 0.40 | 0.37 | 0.39 | 0.34 | 0.35 |
| 2012 | 0.37 | 0.38 | 0.32 | 0.31 | 0.27 | 0.28 | 0.29 | 0.26 | 0.27 | 0.46 | 0.41 | 0.38 | 0.40 | 0.34 | 0.35 |
| 2013 | 0.35 | 0.35 | 0.30 | 0.30 | 0.25 | 0.26 | 0.30 | 0.26 | 0.28 | 0.43 | 0.36 | 0.34 | 0.36 | 0.30 | 0.32 |
| 2014 | 0.29 | 0.32 | 0.28 | 0.25 | 0.22 | 0.24 | 0.25 | 0.24 | 0.26 | 0.37 | 0.33 | 0.30 | 0.33 | 0.29 | 0.32 |
| 2015 | 0.34 | 0.35 | 0.32 | 0.28 | 0.24 | 0.25 | 0.25 | 0.25 | 0.28 | 0.46 | 0.37 | 0.37 | 0.40 | 0.34 | 0.35 |
| 2016 | 0.32 | 0.35 | 0.33 | 0.27 | 0.23 | 0.26 | 0.26 | 0.24 | 0.28 | 0.38 | 0.33 | 0.32 | 0.39 | 0.34 | 0.37 |
| 2017 | 0.33 | 0.36 | 0.33 | 0.28 | 0.25 | 0.27 | 0.26 | 0.25 | 0.27 | 0.39 | 0.36 | 0.35 | 0.38 | 0.37 | 0.36 |
| 2018 | 0.34 | 0.36 | 0.31 | 0.29 | 0.25 | 0.28 | 0.28 | 0.28 | 0.29 | 0.41 | 0.37 | 0.43 | 0.35 | 0.33 | 0.33 |
| 2019 | 0.31 | 0.34 | 0.28 | 0.26 | 0.22 | 0.24 | 0.24 | 0.26 | 0.25 | 0.37 | 0.35 | 0.39 | 0.33 | 0.32 | 0.31 |
| 2020 | 0.28 | 0.32 | 0.25 | 0.24 | 0.21 | 0.23 | 0.23 | 0.23 | 0.23 | 0.35 | 0.32 | 0.35 | 0.34 | 0.32 | 0.30 |
| Mean | 0.34 | 0.36 | 0.31 | 0.27 | 0.24 | 0.25 | 0.28 | 0.26 | 0.27 | 0.41 | 0.36 | 0.35 | 0.37 | 0.33 | 0.34 |
| SD | 0.02 | 0.02 | 0.02 | 0.02 | 0.02 | 0.02 | 0.02 | 0.02 | 0.01 | 0.04 | 0.03 | 0.03 | 0.02 | 0.02 | 0.02 |

of this observation across datasets underscores its reliability. The deviation observed in the surrounding areas of the Sahara Desert in CAMSRA data is attributed to specific regional meteorological conditions or differing data assimilation techniques. Nonetheless, the overall coherence of the observation reaffirms the influence of winter on aerosol dispersion patterns. In the spring season (Fig. 3), the maximum AOD values manifest in the SSD, ME, and CWA regions, due to factors such as wind patterns, land cover, and atmospheric stability interacting to drive aerosol loading during this period (Ridley et al. 2014). The accumulation of aerosols and increased concentration during spring is majorly related to surface heating, atmospheric mixing, long-range transport, and vegetation dynamics (Prospero 1999; Rosenfeld et al. 2008; Huang et al. 2016; Berhane and Bu 2021; Kumar et al. 2018; Boiyo et al. 2017, 2018). The pronounced AOD values observed in the Red Sea region are linked to the prevalence of dust storms and aerosol-rich marine aerosol sources in the vicinity of the region (Saturno et al. 2018; Peshev et al. 2023).

AOD reaches its maximum in the summer as a buildup of aerosols starting from the spring season. The elevated AOD levels observed during summer over regions dominated by desert dust, such as SSD and ME, are by the concept of dust, due to outbreaks driven by increased atmospheric instability and uplift of aerosols induced by the winds (Boiyo et al. 2018; Yu et al. 2018). The identification of the CWA region as a potential hotspot for bioaerosols is supported by its diverse ecological characteristics, including tropical forests, savannas, and proximity to wetlands. These environments contribute to the emission of various types of bioaerosols, such as pollen, fungal spores, plant debris, bacteria, and viruses, which are typical in such biodiverse and humid regions (Li et al. 2016). The contrasting trend in the autumn season, characterized by reduced AOD compared to winter, could result from changing atmospheric circulation patterns and the diminished influence of dust sources due to wet deposition resulting in the removal of particles from the atmosphere and hence settling on the ground (Berhane et al. 2024).

Figure 4a and b depict a comprehensive analysis of the temporal evolution of seasonally and monthly-averaged AOD within the study area from 2003 to 2020. The visualization elucidates negligible fluctuations in AOD, delineating distinctions among datasets sourced from the MODIS, CAMSRA, and MERRA-2. Delineated by intricate dashed lines intersecting with circular dots denoting specific data points, the representation spans all seasons and months, encapsulating the dynamic alterations in AOD over the specified temporal domain. A discernible cyclic pattern in AOD, marked by conspicuous fluctuations across seasons, is revealed in Fig. 4a. Specifically, elevated AOD levels are

observed during certain months, contrasting with reduced levels in others. While the presence of aerosols may be influenced by localized conditions, it is crucial to acknowledge the overarching patterns characteristic of the MENA region, where desert conditions often dominate. The rise in AOD during specific months can be associated with meteorological conditions conducive to aerosol accumulation, including wind patterns transporting aerosol particles into the region. Although relative humidity can play a role in enhancing aerosol growth, as noted by Kumar et al. (2009, 2013), and Boiyo et al. (2018), it is important to recognize that such effects may not uniformly apply across the extensive desert landscapes of the MENA. Previous studies, including He et al. (2008), Alam et al. (2010), and Hu et al. (2018), also highlight the complexity of atmospheric conditions and the role of moisture in influencing aerosol dynamics. Furthermore, while the summertime monsoon can typically reduce aerosol concentrations through wet deposition processes, this effect is not uniformly observed across all regions. In the context of equatorial central Africa, the influence of monsoon precipitation on AOD may vary significantly. This variability is crucial to consider, as the data presented in Fig. 3 indicates enhanced AOD levels during summer across the study domain. The interplay of factors such as regional climatic conditions and aerosol sources shapes the temporal trajectory of AOD, suggesting that changes in AOD may not solely rely on humidity levels or monsoon impacts.

The monthly mean time series plot of AOD data is presented from the three datasets spanning from 2003 to 2020 and is shown in Fig. 4(b). MODIS consistently exhibits higher AOD values than CAMSRA and MERRA-2, primarily during May through September, covering both spring and summer seasons. However, from January to April, MERRA-2 surpassed CAMSRA in AOD magnitude. In the period from September to December, the trajectories of CAMSRA and MERRA-2 are nearly parallel. For example, MODIS recorded an AOD value of 0.44 in July, while CAMSRA and MERRA-2 reported 0.42 and 0.38, respectively. The most significant deviation is observed in July, particularly noticeable in the CAMSRA and MERRA-2 datasets due to variations in retrieval algorithms, data assimilation techniques, or atmospheric conditions specific to that month. These observations suggest that MODIS consistently captures higher AOD values during the warmer months, especially in summer. However, during the rest of the year, MERRA-2 tends to have higher AOD values compared to CAMSRA. This variability underscores the importance of considering multiple datasets and their potential biases when analyzing AOD data (Boiyo et al. 2017; Ali et al. 2022).

Figure 5A demonstrates the validation of AOD, showing good consistency and strong positive coefficients of

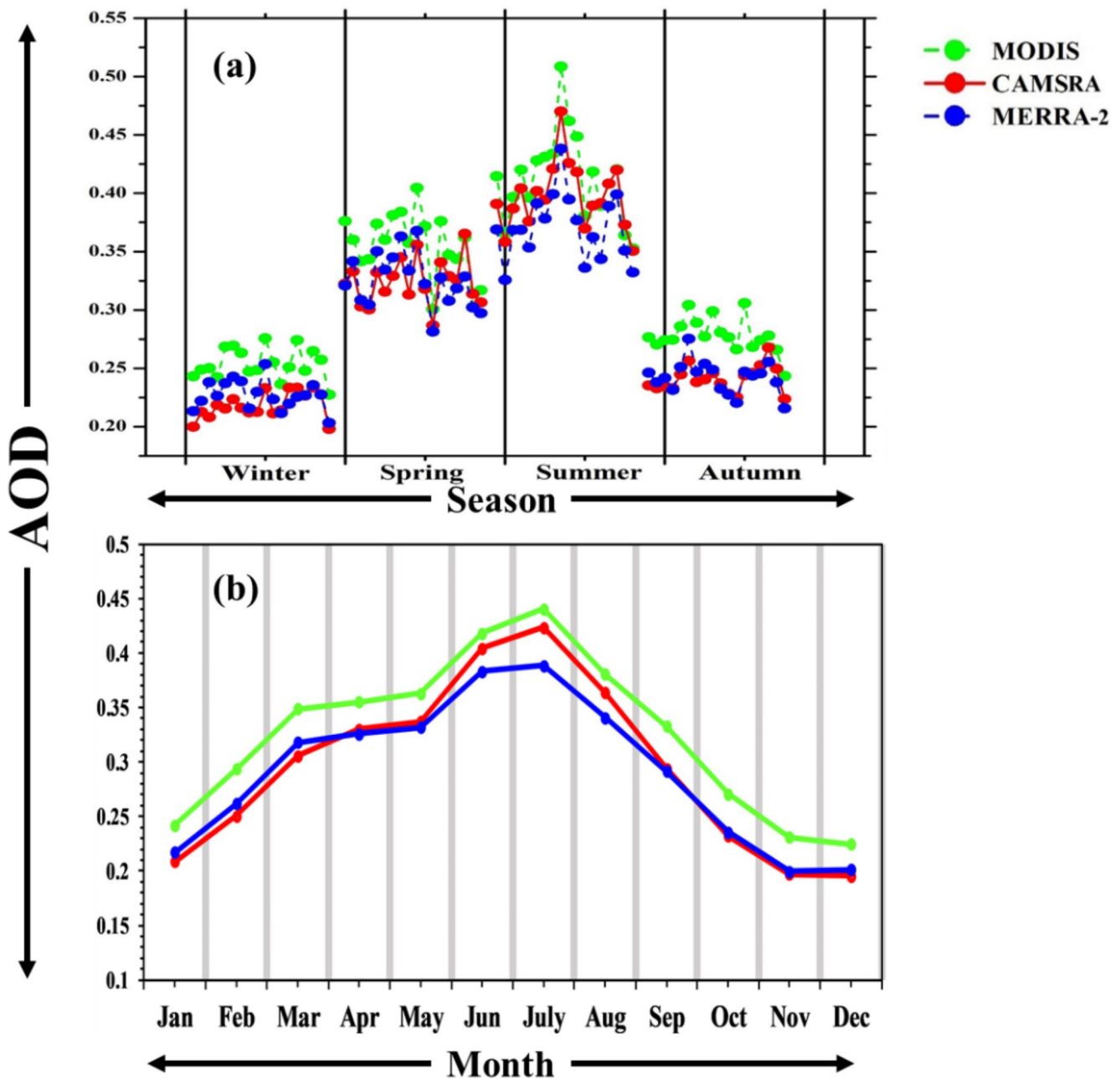


Fig. 4 Seasonal (a) and monthly (b) time series AOD patterns over the study domain averaged from 2003 to 2020, derived from MODIS, CAMSRA, and MERRA-2

determination (R^2) between MODIS and CAMSRA for each season. The R^2 values for DJF, MAM, JJA, and SON are 0.943, 0.767, 0.954, and 0.946, respectively. Similarly, Fig. 5B highlights the comparison between MODIS and MERRA-2, with strong R^2 values of 0.934, 0.858, 0.908, and 0.962 for DJF, MAM, JJA, and SON, respectively. These results affirm the coherence of the datasets in the study region. The comparison highlights the ability of the datasets to capture seasonal variations in AOD, reinforcing the reliability of remote sensing products. Both CAMSRA

and MERRA-2 datasets benefit from advanced data assimilation techniques and improved retrieval algorithms, which enhance accuracy in AOD measurements. However, contextual factors like atmospheric variations and algorithm assumptions should be considered, acknowledging uncertainties despite the robust correlations.

The histogram plots of the three datasets and the anomalies within them are visually represented for the interannual AOD_{550} in Fig. 6a and b. In Fig. 6a, the interannual manifestation of AOD_{550} across the three datasets indicates

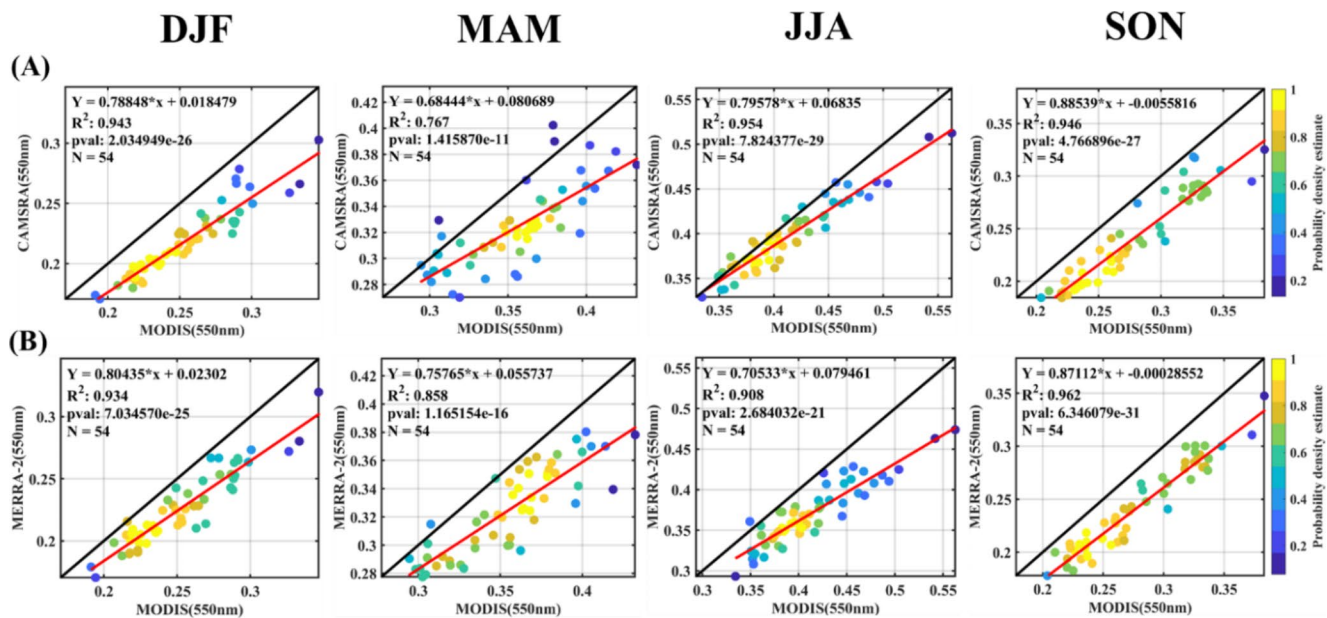


Fig. 5 Seasonal scatter plots of AOD between (A) CAMSRA versus MODIS, and (B) MODIS versus MERRA-2 represent the inter-comparison between the satellite datasets over the entire study region from 2003 to 2020

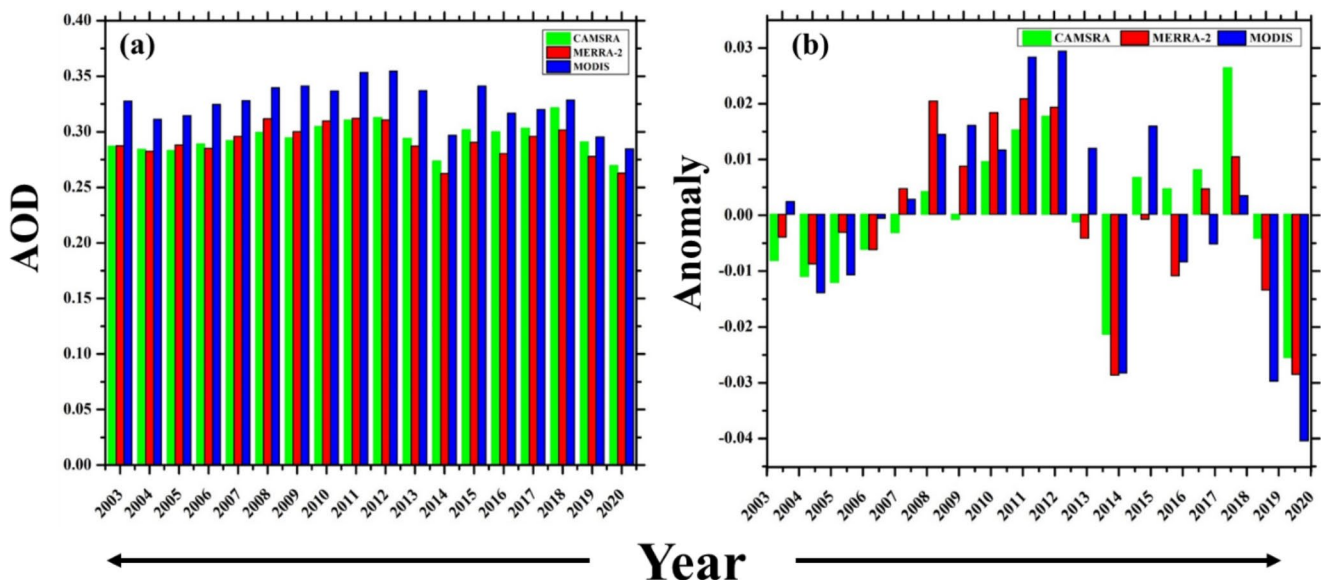


Fig. 6 Time series of (a) yearly mean and (b) yearly mean anomalies of AOD over the entire study domain during 2003–2020 from CAMSRA, MODIS, and MERRA-2. The anomalies correspond to the averaged values of 2003–2020 for each dataset

an escalation in values, in 2011 and 2012, and minimum observed in 2014 and 2020. Conversely, the AOD data sourced from the CAMSRA and MERRA-2 datasets exhibit analogous trends, distinguished by marginal disparities when compared with the MODIS AOD dataset. It is unveiled that the maximum annual mean AOD across all three datasets within the study region occurred in 2012, encompassing the distinct heterogeneity over the study domain. Substantial decreases are evident from 2012 to 2014 and from 2018 to 2020. Consistency is observed in the patterns exhibited

by the three datasets, with the MODIS presenting magnitudes of greater amplitude relative to the lower magnitudes observed in MERRA-2. The sudden fluctuations in AOD in the MENA region are primarily driven by a complex interplay of meteorological, environmental, and anthropogenic factors. Wind speed is the dominant meteorological influence, explaining up to 30.3% of AOD variance in mineral-dust-dominant areas, while humidity plays a crucial role in biomass-burning regions (Kunchala et al. 2024). The MENA region's susceptibility to frequent and intense dust storms,

originating from sources like the Arabian Peninsula and North Africa, significantly impacts AOD levels. Anthropogenic activities, including urban emissions and agricultural burning, contribute to short-term AOD spikes. Seasonal patterns, with higher AOD values typically observed during the spring and summer seasons, further complicate the picture (Karami et al. 2024). Additionally, long-term trends and potential reversals in AOD, like those observed in other regions of East China, may occur due to changes in source emissions or meteorological patterns. This multifaceted interaction of factors results in the dynamic and often unpredictable AOD fluctuations characteristic of the MENA region (Shaheen et al. 2020; Rocha-Lima et al. 2024). Also, the findings from Klingmuller et al. (2016) highlighted how prolonged drought conditions, particularly in the Middle East, significantly affected dust emissions due to reduced soil moisture. This phenomenon was especially notable during the prolonged drought period from 2008 to 2012, which saw a marked increase in dust emissions. In this study, the variability in AOD over the region is linked to such climatic conditions, with specific emphasis on seasons influenced by these prolonged dry periods. By focusing on the temporal and spatial nuances of drought-induced dust emissions, we aim to provide a more detailed understanding of how these conditions affect AOD variability, particularly in regions prone to prolonged dry spells.

Figure 6b illustrates the yearly AOD anomalies from CAMSRA, MODIS, and MERRA-2 during the period 2003–2020. These anomalies highlight several significant trends. First, the negative anomalies from 2003 to 2007 can be linked to lower emissions of dust and aerosols during those years, possibly due to favorable meteorological conditions such as reduced drought severity or lower wind speeds in the region. The inflection point in 2008 marks a period of increasing aerosol emissions, which could be associated with intensified dust storms and other anthropogenic factors, especially as the region experienced prolonged droughts between 2008 and 2012 (Notaro et al. 2015; Hamzeh et al. 2021). The peak anomaly in 2012 is consistent with these

dust emission events exacerbated by drought conditions. In contrast, 2020 shows a steep decline in AOD anomalies across all datasets, with MODIS displaying the most prominent negative anomaly. This sharp decrease might be attributed to a combination of factors, including the reduction of human activities due to the COVID-19 pandemic and changing meteorological conditions that limited dust transport during that year.

3.3 Spatiotemporal Variations and Contributions of AOD for each Aerosol Species

Table 3 provides a comprehensive set of statistical metrics for each aerosol species from 2003 to 2020. The data analysis unveiled a conspicuous predominance of dust across the diverse aerosol datasets, followed by sulfate, organic carbon (OC), sea salt, and black carbon (BC). Employing the Mann-Kendall (MK) trend test, it is discerned that BC and OC exhibit a discernible positive trend, signifying an increasing trend. In contrast, the remaining aerosol species indicate no discernible alterations in their trends. This emergent trend, particularly in BC and OC concentrations, might serve as an indicative signal of escalating anthropogenic activities, posing potential environmental and health hazards. Notably, an intriguing antagonistic behavior between the two datasets is observed in the BC, suggesting a subtle relationship that necessitates scrutiny. Consequently, these divergent observations underscore the imperative for a more sophisticated approach and thorough evaluative considerations to reconcile and elucidate the underlying causes of such disparities in the datasets.

Figure 7 presents the monthly analysis of AOD for the five different aerosol species based on both CAMSRA and MERRA-2 datasets. The corresponding standard deviations and AOD percentages within the study region are also included. Also, Table 4 displays the statistical values of seasonal mean AOD for the five aerosol species observed in the study area. Table 4 reveals some disparities in the mean AOD values obtained from each dataset over each season.

Table 3 Comparative analysis of annual extremes, variability (\pm SD), and Mann-Kendall (MK) trend test results at a 95% confidence level (with H and P-Values provided) for AOD across various aerosol species derived from the CAMSRA and MERRA-2 datasets for the study region from 2003 to 2020. Subscripts C and M denote CAMSRA and MERRA-2, respectively

| | Min | Max | Mean | SD. | Slope (m) | H | P-value | MK-Trend Test Result |
|------------|-------|-------|-------|-------|-----------|-------|---------|----------------------|
| BC_C | 0.005 | 0.019 | 0.010 | 0.002 | -1285.4 | 0.000 | 0.423 | Insignificant |
| BC_M | 0.005 | 0.014 | 0.009 | 0.002 | 4862.6 | 1.000 | 0.028 | Significant |
| Dust_C | 0.041 | 0.233 | 0.126 | 0.053 | -2.8 | 0.000 | 0.978 | Insignificant |
| Dust_M | 0.079 | 0.324 | 0.183 | 0.063 | -100.5 | 0.000 | 0.064 | Insignificant |
| OM_C | 0.057 | 0.142 | 0.086 | 0.017 | 362.0 | 0.000 | 0.071 | Insignificant |
| OC_M | 0.014 | 0.051 | 0.029 | 0.009 | 1812.8 | 1.000 | 0.000 | Significant |
| Sea-Salt_C | 0.004 | 0.022 | 0.010 | 0.004 | -564.9 | 0.000 | 0.968 | Insignificant |
| Sea-Salt_M | 0.011 | 0.040 | 0.021 | 0.007 | -98.4 | 0.000 | 0.679 | Insignificant |
| Sulfate_C | 0.039 | 0.116 | 0.064 | 0.017 | 27.8 | 0.000 | 0.704 | Insignificant |
| Sulfate_M | 0.026 | 0.094 | 0.050 | 0.016 | -213.1 | 0.000 | 0.300 | Insignificant |

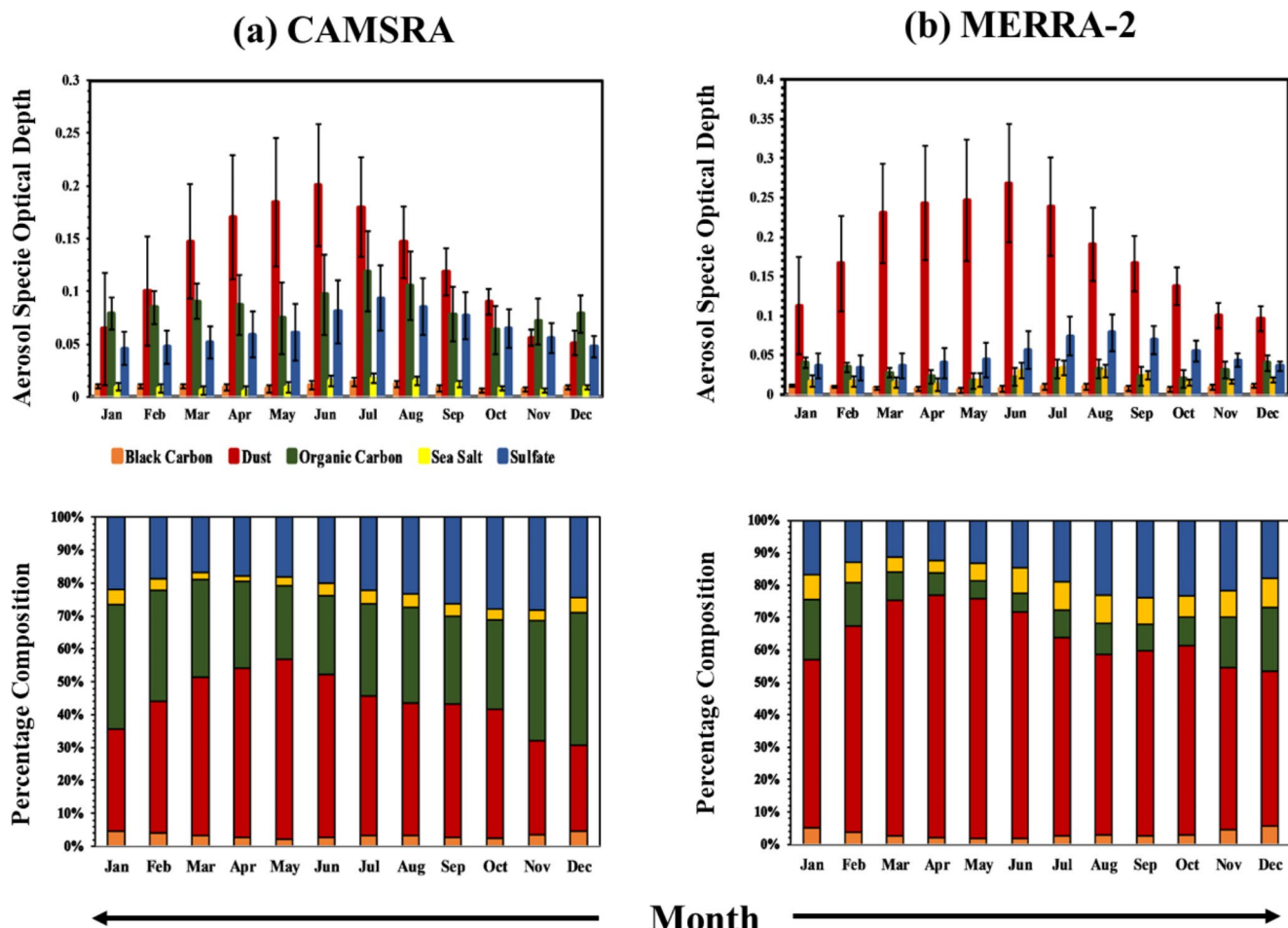


Fig. 7 Monthly mean AOD of five aerosol species and their percentages over the study area during 2003–2020 from (a) CAMSRA (left panels both top and bottom) and (b) MERRA-2 (right panels both top

and bottom). The thin and short vertical lines represent the standard deviation for each aerosol species

Table 4 Seasonal-mean AOD across various aerosol species from the CAMSRA and MERRA-2 datasets over the study region during 2003–2020

| | DJF | | MAM | | JJA | | SON | |
|----------------|--------|---------|--------|---------|--------|---------|--------|---------|
| | CAMSRA | MERRA-2 | CAMSRA | MERRA-2 | CAMSRA | MERRA-2 | CAMSRA | MERRA-2 |
| Black Carbon | 0.010 | 0.011 | 0.009 | 0.007 | 0.012 | 0.009 | 0.007 | 0.158 |
| Dust | 0.084 | 0.142 | 0.191 | 0.277 | 0.196 | 0.265 | 0.103 | 0.008 |
| Organic Carbon | 0.078 | 0.038 | 0.081 | 0.022 | 0.106 | 0.029 | 0.068 | 0.024 |
| Sea-salt | 0.007 | 0.012 | 0.005 | 0.012 | 0.008 | 0.020 | 0.006 | 0.015 |
| Sulfate | 0.044 | 0.033 | 0.054 | 0.036 | 0.085 | 0.071 | 0.066 | 0.056 |

Notably, BC exhibits non-uniform values, with greater consistency during winter (DJF) and summer (JJA). In contrast, Dust shows elevated values during spring (MAM) and summer (JJA) in the MERRA-2 dataset. However, unlike Dust, the CAMSRA data indicates higher magnitudes than MERRA-2. Whereas, OC dominates the winter season. AOD from Sea-Salt aerosols displays distribution patterns rather than distinct seasonal variations. Furthermore, Sulfate concentrations are more prominent during summer and autumn. Dust holds the highest abundance, followed by OC, Sulfate, BC, and sea salt, as observed in the CAMSRA data

(Fig. 7a). Standard deviation within the CAMSRA data fluctuates, with Dust exhibiting the highest variability ranging between 0.02 and 0.12. Following Dust, OC has the second-highest standard deviation ranging from 0.0 to 0.048. The standard deviation ranges between 0.01 and 0.05 for each aerosol species. Similar to CAMSRA, the percentage change in AOD from MERRA-2 shows differences in mean AOD for similar aerosol types. Strong standard deviation values in MERRA-2 correspond to Dust aerosol composition, like CAMSRA.

Sulfate aerosol standard deviation ranges from 0.02 to 0.05 in MERRA-2, ranking as the second highest, unlike the CAMSRA where it is the third highest. The monthly analysis indicates dust as the dominant aerosol component in both CAMSRA and MERRA-2 datasets, with percentages of 55% and 75% respectively. Dust increases from January, peaks around April and May, and then decreases. OC ranks as the second-highest aerosol component in CAMSRA data, while Sulfate takes this place in MERRA-2. OC values peak at the beginning and end of the year and dip around the middle. Sulfate displays varying rankings and an increasing trend until August and September, followed by a decline. The percentages of aerosol types vary between the datasets. For instance, OC ranges from 40 to 23% in CAMSRA and 18–6% in MERRA-2. Sulfate ranges from 25 to 18% in CAMSRA and 25–12% in MERRA-2. Sea-salt concentrations exceed BC in both datasets, with Sea-Salt accounting for 4–0.5% and 7–3%, while BC remains consistent. Hence, the study region predominantly experiences Dust aerosols due to its desert characteristics. Anthropogenic aerosols have an observable impact despite the dominance of dust aerosols. OC and Sulfate aerosols prevail, particularly from April to June when Dust aerosols peak over the domain. The discrepancy in aerosol rankings between CAMSRA and MERRA-2 datasets for the MENA region, particularly regarding organic carbon and sulfate, stems from differences in model formulations, emission inventories, and chemical schemes. While both datasets agree on dust dominance, CAMSRA may be capturing more organic carbon sources or underestimating sulfate levels compared to MERRA-2. This variation underscores the uncertainties in aerosol modeling and the importance of using multiple datasets and ground-based measurements for comprehensive assessments (Mortier et al. 2020; Thompson and Zakhirova 2021; Zhong et al. 2022). Outside this period, OC and Sulfate increase with the decrease of Dust aerosols. This trend extends to sea salt and BC aerosols as well.

As depicted in Fig. 8, the analysis of AOD anomalies distinctly illustrates inter-annual variations among the five aerosol species considered within this study over the entire study domain from 2003 to 2020. Variations in aerosol concentrations occur annually and are distinctive for each aerosol type. It is noteworthy that aerosols like Black Carbon, which are infrequently found in the study region, show significant discrepancies between the MERRA-2 and CAMSRA datasets. This observation underscores that BC, OC, and Sulfates exhibited higher levels in 2011, 2012, 2013, 2016, and 2017. Conversely, they were generally lower during 2003, with intermittent exceptions extending until 2009. Notably, Sulfate was noticed lower in 2004. Meanwhile, Dust and Sea Salt demonstrated negative anomalies in 2014,

2019, and 2020. According to the CAMSRA data, a negative anomaly for Sea Salt emerged in the year 2018.

The correlation analysis between the five aerosol species taking the two datasets as frames of reference is also of great interest and value because the aerosols exhibit temporal fluctuations over the period. Figure 9 shows the correlation between MERRA-2 and CAMSRA datasets for all species of aerosols from 2003 to 2020 across the entire study domain. While Black Carbon data points mostly align along the 1:1 line, indicating relatively good agreement between MERRA-2 and CAMSRA. However, this is not the case for Dust and Sea Salt aerosols. These two species are systematically overestimated in the MERRA-2 dataset, despite high R^2 values, which might misleadingly suggest good consistency between the datasets. This overestimation highlights that the coefficient of determination (R^2) alone should not be used as the sole metric for evaluating dataset agreement. The results indicate an R^2 value of 0.432 for BC, which shows moderate agreement, while Organic Carbon (OC) aerosols exhibit a lower correlation ($R^2 = 0.269$), reflecting more significant discrepancies between the two datasets. For Dust ($R^2 = 0.97$), Sea Salt ($R^2 = 0.941$), and Sulfate ($R^2 = 0.892$), the correlation analysis shows high R^2 values, but this should not obscure the fact that there are systematic biases, especially for Dust and Sea Salt. Therefore, while the R^2 is strong, the overestimation of these aerosol species in the MERRA-2 dataset indicates that the agreement between MERRA-2 and CAMSRA is not as robust as the high R^2 values.

Table 5 provides a detailed breakdown, expressed in percentages, of the seasonal composition of five distinct aerosol species within the study area. Figure 10 provides a visually compelling representation, revealing the intricate distribution of aerosols categorized as BC and Dust types across the entire study area. These insightful findings are derived from both the CAMSRA (C) and MERRA-2 (M) datasets, adding a layer of depth to the analysis. The careful delineation of the study area emphasizes the profound importance of exploring the spatial concentration intricacies exhibited by the quintet of aerosol species, each intricately linked to a specific geographical expanse. Notably, the percentage of Dust is comparatively lower than other aerosol species due to its widespread distribution across the region. Major Dust aerosols are prevalent over the North Africa and the Middle East regions, encompassing nearly 70% of the study area. Geographical features like mountains, valleys, coastlines, and proximity to water bodies significantly influence local weather patterns, air circulation, and aerosol dispersion (Liu et al. 2021). These features create diverse aerosol behaviors in different areas. Meteorological conditions, driven by seasonal variations, further shape aerosol behavior. The five aerosol species discussed exhibit varying sources and

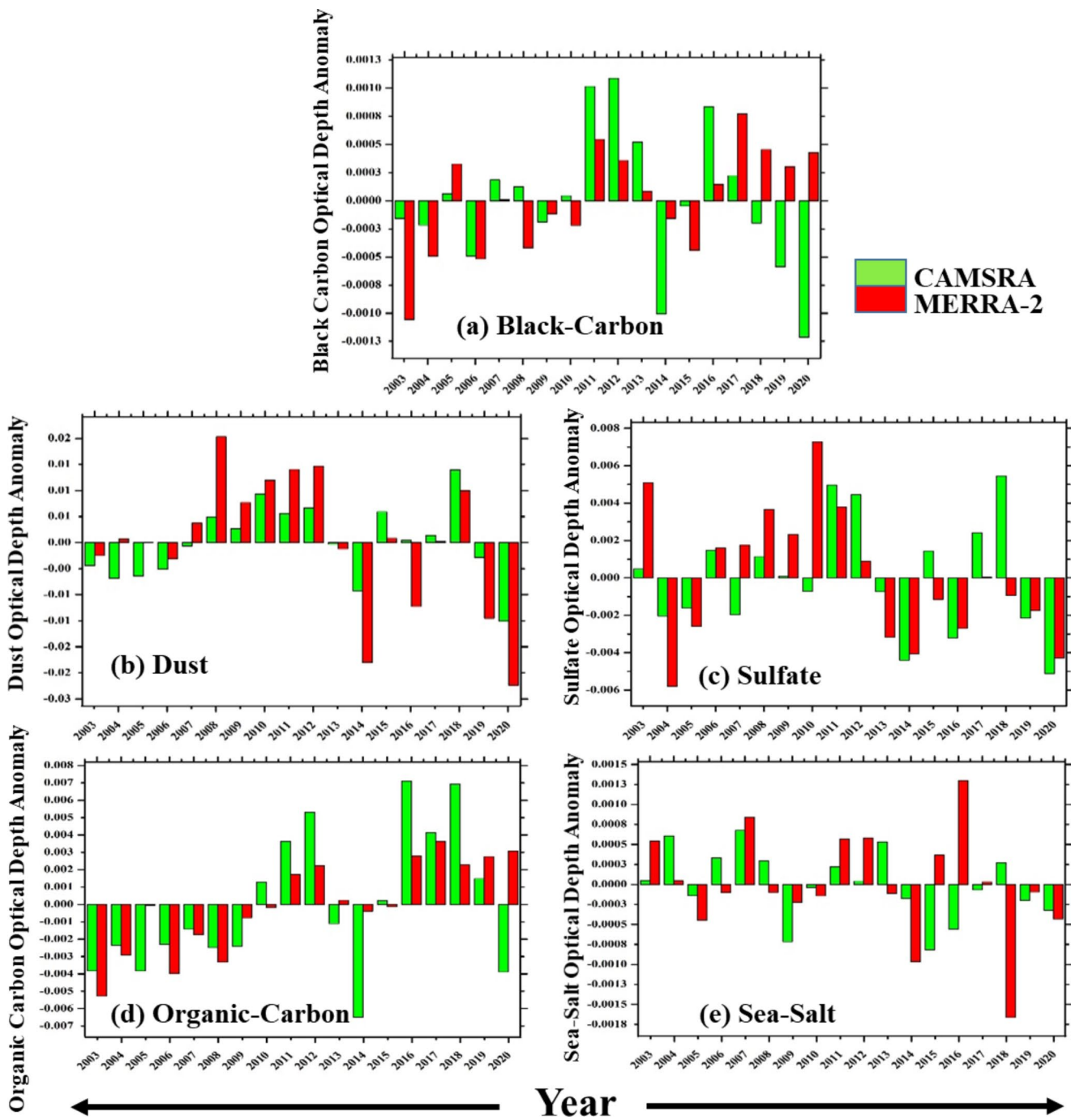


Fig. 8 Inter-annual AOD anomalies of five aerosol species over the study area from the CAMSRA and MERRA-2 datasets during 2003–2020

behaviors throughout the year. These seasonal variations provide vital insights into aerosol dissemination.

Notably, BC aerosols showed high values throughout the year in the CWA region, primarily due to biomass burning, agricultural residue burning, and indoor cooking using solid fuels (Capes et al. 2008; Yu et al. 2013) (Fig. 10; Table 5). Even during warmer seasons, significant BC levels persist, suggesting contributions from vehicular emissions and open biomass burning. Dust aerosols, originating

from arid regions, play a pivotal role year-round. The data in Table 5 and the MERRA-2 dataset confirm their dominance. Primary sources include the Sahara Desert (from the SSD region) and the Arabian Desert (Fig. 10). The spring and summer seasons experienced over 80% coverage of dust aerosols, driven by regional wind patterns and local sources. However, certain areas in East, West, and Central Africa show deviations, suggesting distinct influences from localized sources. Regardless, dust maintains dominance,

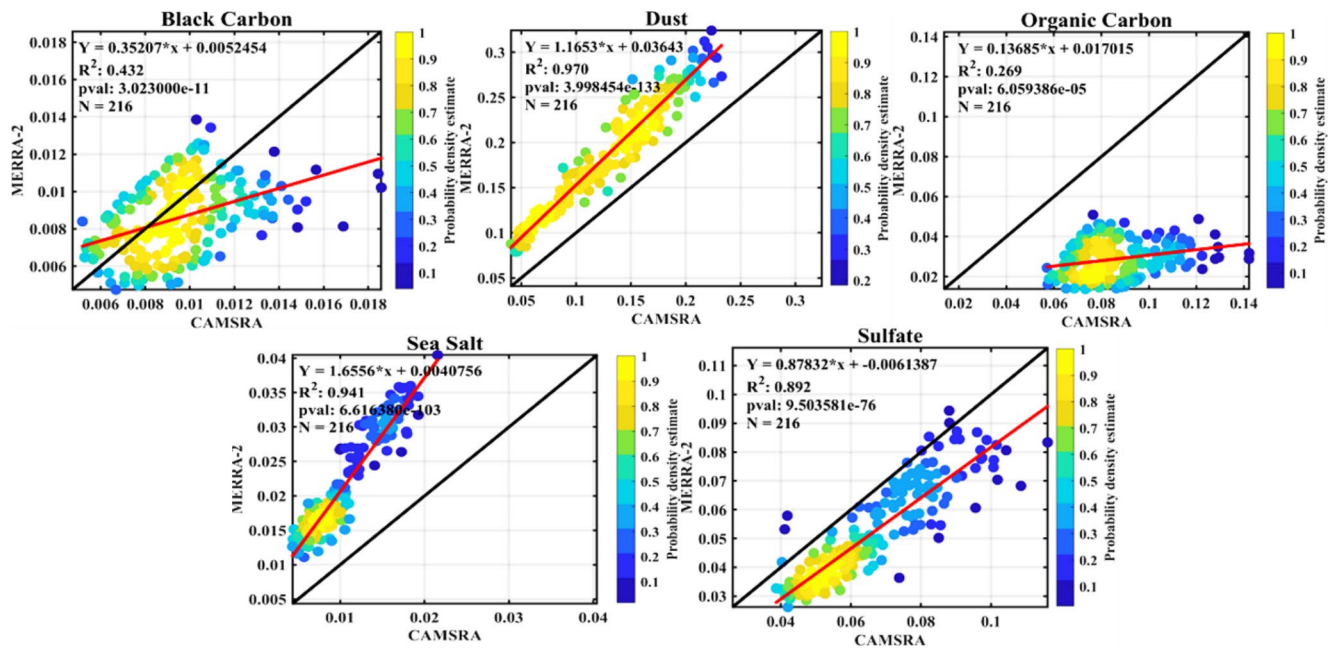


Fig. 9 Scatter plot of the five aerosol species between MERRA-2 and CAMSRA products over the entire study region from 2003 to 2020

Table 5 Seasonal percentage composition of the five aerosol species within each region numbered from one (1) to five (5). Bolded numbers represent the highest amount from each of the datasets

| Season | Region | Black Carbon (%) | | Dust (%) | | Organic Carbon (%) | | Sea-Salt (%) | | Sulfate (%) | |
|--------|--------|------------------|--------------|--------------|--------------|--------------------|--------------|--------------|--------------|--------------|--------------|
| | | M | C | M | C | M | C | M | C | M | C |
| DJF | SSD | 11.58 | 12.53 | 19.3 | 18.6 | 9.12 | 10.24 | 12.02 | 11.25 | 47.98 | 47.38 |
| | EA | 22.76 | 26.25 | 11.23 | 8.32 | 17.04 | 21.73 | 20.88 | 22.88 | 28.09 | 20.82 |
| | NA | 9.06 | 10.34 | 19.74 | 19.65 | 6.32 | 10.88 | 8.31 | 13.18 | 56.58 | 13.18 |
| | ME | 16.59 | 18.03 | 42.59 | 25.22 | 13.66 | 32.24 | 19.31 | 15.35 | 7.86 | 9.16 |
| | CWA | 13.98 | 16.64 | 19.12 | 17.1 | 17.57 | 20.04 | 32 | 35.69 | 17.34 | 10.53 |
| MAM | SSD | 16 | 15.29 | 19.51 | 17.49 | 17.81 | 17.81 | 19.73 | 20.05 | 26.95 | 29.36 |
| | EA | 25.22 | 25.28 | 9.39 | 6.94 | 21.2 | 24.04 | 22.42 | 24.8 | 21.76 | 18.94 |
| | NA | 11.71 | 11.82 | 22.96 | 20.78 | 12.59 | 14.14 | 15.23 | 18.91 | 37.51 | 34.35 |
| | ME | 13.97 | 11.7 | 40.89 | 37.5 | 12.47 | 20.49 | 23.97 | 14.62 | 8.7 | 15.68 |
| | CWA | 13.36 | 13.81 | 20.79 | 18.67 | 17.89 | 16.71 | 33.74 | 35.55 | 14.22 | 15.26 |
| JJA | SSD | 15.91 | 13.74 | 17.13 | 18.3 | 16.5 | 16.89 | 20.59 | 17.6 | 29.87 | 33.46 |
| | EA | 28.79 | 28.97 | 15.64 | 14.57 | 14.87 | 17.15 | 27.54 | 26.76 | 13.16 | 12.55 |
| | NA | 10.43 | 12.22 | 21 | 21.95 | 8.53 | 13 | 11.91 | 16.7 | 48.13 | 36.14 |
| | ME | 13.81 | 6.03 | 31.75 | 56.06 | 14.91 | 7.15 | 33.68 | 16.64 | 5.84 | 14.12 |
| | CWA | 20.82 | 15.86 | 23.47 | 25.6 | 16.4 | 16.02 | 24.05 | 25.23 | 15.26 | 17.28 |
| SON | SSD | 15.27 | 16.1 | 19.72 | 20.89 | 13.97 | 17.31 | 21.09 | 17.18 | 29.95 | 28.52 |
| | EA | 29.29 | 31.12 | 11.17 | 9.34 | 19.48 | 22 | 22.53 | 21.15 | 17.53 | 16.39 |
| | NA | 10.21 | 12.72 | 22.76 | 24.04 | 8.07 | 14.17 | 12.63 | 17.22 | 46.34 | 31.86 |
| | ME | 19.11 | 9.67 | 33.97 | 41.55 | 16.32 | 19.32 | 22.55 | 10.41 | 8.05 | 16.05 |
| | CWA | 18.88 | 18.98 | 20.07 | 20.16 | 17.18 | 19.15 | 28.1 | 27.23 | 15.77 | 14.48 |

especially in the SSD region due to its atmospheric dynamics with limited vegetation and strong winds, facilitating continuous dust generation and transport.

Figure 11 displays the distributions of OC and Sea-salt aerosols, while Table 5 provides detailed statistics of aerosol species. Both datasets reveal a clear pattern: OC concentrations peak in the CWA region during specific periods,

as confirmed by MERRA-2 data (Yoon et al. 2007). Figure 11 also shows Sea-salt aerosols concentrated near the Red Sea and surrounding coasts, influenced by the region's unique dynamics (Liu et al. 2005; Textor et al. 2006; Prijith et al. 2014). The seasonal variations in OC concentrations are driven by a combination of meteorological conditions, human activities, and biogenic emissions. During winter,

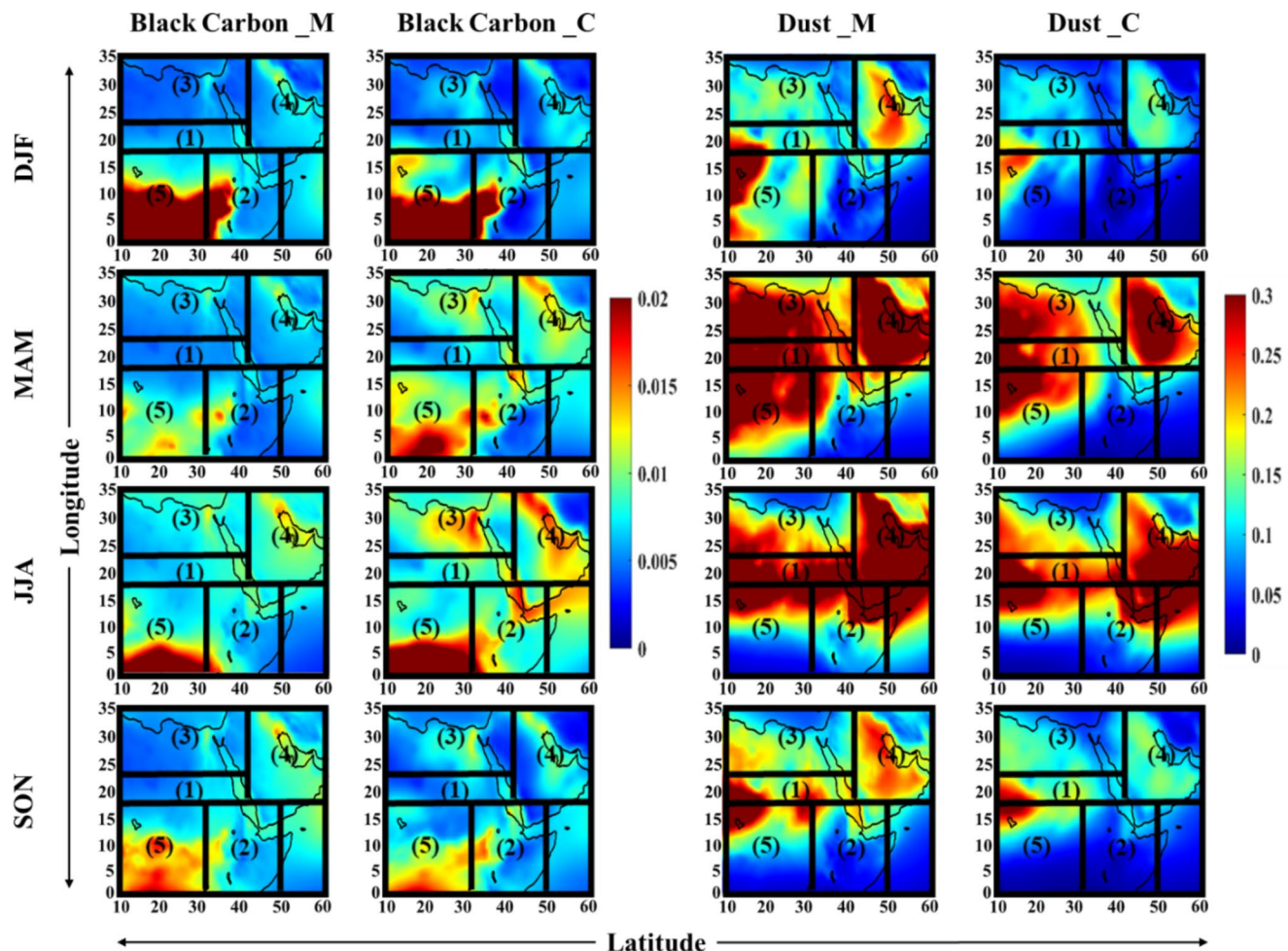


Fig. 10 Spatial distributions of Black Carbon and Dust from MERRA-2 (M) and CAMSRA (C) products over the entire study region during 2013–2020. The subscripts M and C represent MERRA-2 and CAMSRA, respectively

stable atmospheric conditions, temperature inversions, and reduced vertical mixing contribute to the buildup of OC levels. These increases are often due to biomass burning, agricultural residue burning, and residential cooking using solid fuels rather than heating (Yoon et al. 2007). Notably, unlike regions such as North India, where winter combustion emissions stem from heating purposes (Ganguly et al. 2006), the CWA region experiences combustion emissions primarily from cooking and other household activities during this season. In summer, higher temperatures and enhanced biogenic activity result in a rise in OC levels, further driven by increased biomass burning.

The presence of Sea-salt aerosols in the Red Sea region is attributed to oceanic and air-sea interactions, where wind-driven processes fragment seawater droplets into sea salts, subsequently influenced by prevailing winds (Gong et al. 1997). The extensive water surface of the nearby Indian Ocean also fosters the generation of sea-salt aerosols due to strong winds and turbulence, and these aerosols are transported across the study area by atmospheric circulation.

Understanding the spatial distributions of OC and Sea-salt aerosols, along with their connections to meteorological and geographical factors, provides valuable insights into the complex interplay of natural and human-induced processes shaping the atmospheric composition in the CWA region.

Figure 12 depicts the spatial distribution of sulfate aerosol types using comprehensive datasets. Sulfate aerosol concentrations are notably elevated around the Red Sea and the ME, necessitating scientific explanation due to various meteorological and geographical factors in these regions. One plausible reason for increased sulfate aerosols is the influence of nearby industrialized zones and urban centers. These areas likely emit precursor gases like sulfur dioxide (SO_2), which undergo atmospheric oxidation processes, forming sulfate aerosols (Shahid et al. 2021). Anthropogenic activities, including industrial processes and vehicular emissions, significantly contribute to atmospheric SO_2 levels. Local meteorological conditions also exacerbate the accumulation of sulfate aerosols. The coastal regions exhibit distinct wind patterns that converge air masses laden

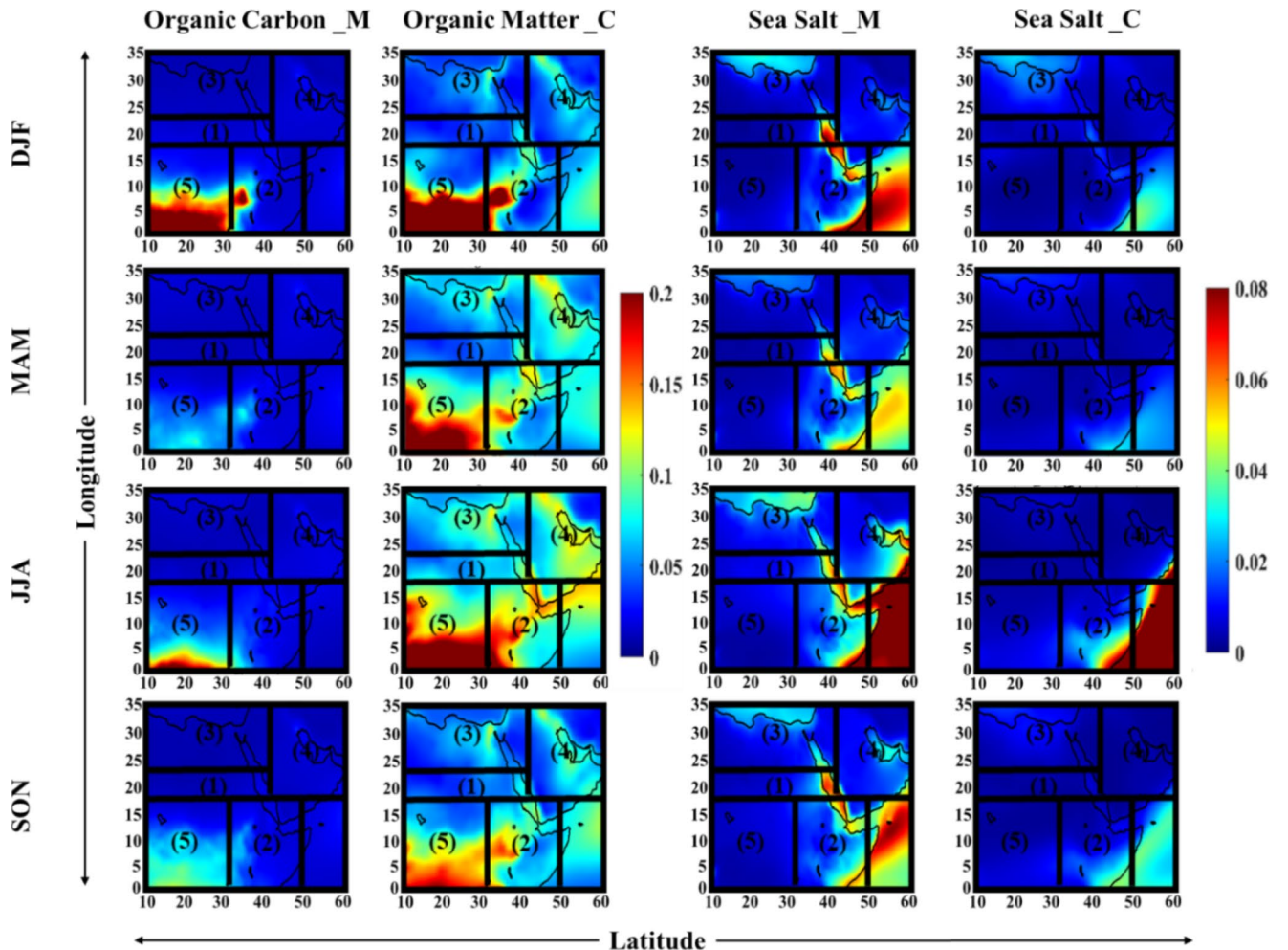


Fig. 11 Same as in Fig. 10, but for the Organic Carbon and Sea Salt

with pollutants. Geographical features trap pollutants, such as sulfate aerosols, leading to higher concentrations (Textor et al. 2006). Moreover, arid environments and desert dust enhance sulfate aerosol formation through reactions on dust particle surfaces (Mahowald et al. 2014; Huang et al. 2014). The seasonal variations, with elevated sulfate concentrations in the spring and summer seasons (Table 5), are due to changes in meteorology and aerosol chemistry (Hu et al. 2018). Warmer seasons promote photochemical reactions, oxidizing sulfur dioxide to sulfate aerosols (Andreae and Rosenfeld 2008; Prospero et al. 2021). Increased solar radiation and temperature affect atmospheric stability and favor aerosol transport (Guleria et al. 2014). The intricate sulfate aerosol distribution, especially around the Red Sea and the Middle East, results from a complex interplay of factors.

Sulfate aerosols are majorly situated within the ME region during DJF with 34% composition on average of both the MERRA-2 and CAMSRA datasets. During MAM, similar to the case of DJF the ME region accounts for the most abundant percentage composition of Sulfate aerosols

with 34% composition on average record. It can be observed from Table 5 that Sulfate aerosols are more abundant during DJF and MAM season. Sulfate aerosols are abundant during the DJF and MAM seasons in the Middle East due to specific atmospheric conditions and processes. The presence of sulfate aerosols is influenced by factors such as secondary production of sulfate via oxidation of sulfur dioxide (SO_2) or dimethyl sulfide (DMS) convectively lifted to the atmosphere. These processes lead to higher surface concentrations of sulfate during DJF and MAM despite sulfate exhibiting higher AODs in other seasons like JJA.

During JJA the Sulfate aerosols recorded 25% abundance in the EA region according to the CAMSRA data while MERRA-2 recorded 24% abundance giving credit to the ME region like the other seasons. With the onset of the discrepancies between the two datasets as explained above the higher abundance of sulfate aerosols in the Middle East region attributed to industrial activities, particularly the burning of fossil fuels like coal and oil, which release sulfur dioxide into the atmosphere. Additionally, the presence

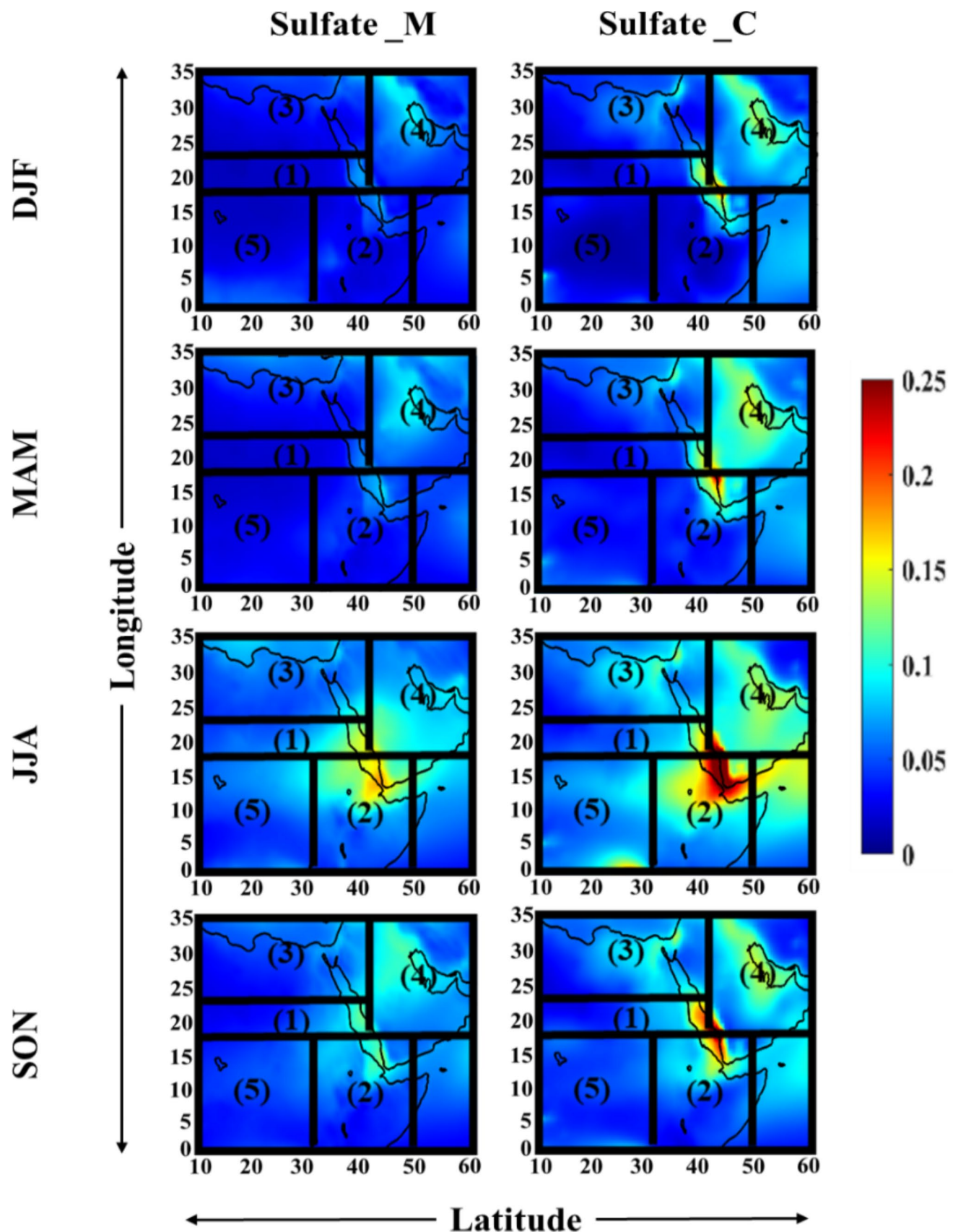


Fig. 12 Same as in Fig. 10, but for the Sulfate

of major industrial zones and urban areas in the Middle East contributes to higher sulfate aerosol concentrations. Furthermore, the geographical location of the Middle East region plays a role in this difference. The region's proximity to major shipping routes and oil refineries can lead to increased emissions of sulfur compounds that contribute to sulfate aerosol formation. In contrast, other regions like East Africa, Sahel Sahara Desert, North Africa, and CWA may have lower sulfate aerosol levels due to fewer industrial activities and different atmospheric conditions. During the SON season, the Sulfate aerosol composition reaches up to 27% in the ME region like the other seasons.

3.4 XGBoost Model Performance on AOD

Figure 13a shows the relationship between the actual and predicted AOD values based on the XGBoost model over the MENA region from 2003 to 2020. The AI/ML-driven XGBoost model demonstrates strong predictive accuracy, with a high correlation coefficient (r) of 0.96, indicating that the predicted AOD values closely follow the actual observations. The Root Mean Square Error (RMSE) of 0.02 is impressively low, suggesting that the model has minimal error in its predictions. Additionally, the mean bias error of the correlation reflects that there is no systematic bias, meaning the model neither over-predicts nor under-predicts the AOD values. The linear fit ($y = 0.94x + 0.01$) closely aligns with the ideal fit, further validating the model's ability to predict AOD. This high level of agreement between actual and predicted AOD values shows that the XGBoost model is well-suited for studying aerosol optical properties in the MENA region. The feature importance plot represents the F-score (Fig. 13b) illustrating the relative influence of different aerosol species on AOD predictions. The most significant contributor to the model's predictions is black carbon, with an F score of 391.0. This reflects its significance and key role in atmospheric opacity and pollution, especially in regions with heavy industrial activities and fossil fuel combustion. Following the BC aerosol, Dust depicts an F score of 337.0, which is the second most critical feature. This is consistent with the frequent dust storms and vast desert areas in the MENA region and is consistent with the previous results shown in this work. Sea salt, contributing a score of 233.0, is an essential factor, especially in coastal areas influenced by marine aerosols. Sulphates and organic carbon, with F scores of 199.0 and 128.0 respectively, represent emissions from industrial activities and biomass burning. The overall feature ranking highlights the importance of both natural and anthropogenic sources in driving AOD levels across the region, with black carbon and dust being the dominant factors.

Also, the SHAP value plot (Fig. 13c) offers a detailed view of how individual features impact the XGBoost model's predictions for AOD. Each dot represents a data point, and the SHAP values show whether the feature contributes positively or negatively to the predicted AOD. The most notable feature is that the dust and sea salt aerosols have predominantly positive SHAP values. This indicates higher concentrations of these aerosols lead to an increase in AOD. This finding is aligned with the geographical characteristics of the MENA region, where dust storms and oceanic aerosol sources are common. Black carbon shows a more complex pattern with both positive and negative SHAP values. This suggests that the increase of BC generally increases AOD, and its impact varies depending on other atmospheric conditions. Sulphate and organic carbon also display a range of SHAP values, indicating their nuanced influence on AOD. The color gradient in the plot, from blue (low feature value) to pink (high feature value), further helps to visualize how changes in feature values affect AOD predictions. This detailed SHAP analysis reveals the complex interplay between different aerosol types and their contributions to AOD in the region.

4 Summary of Conclusions

The present study examines a comprehensive evaluation and analysis of AOD over the Middle East and North Africa (MENA) region using MERRA-2 and CAMSRA reanalysis datasets, with MODIS data as the reference. The analysis spans from 2003 to 2020, focusing on various regions of MENA with distinct climatic conditions. The MENA region is known for diverse sources of both natural and anthropogenic aerosols, and the study includes five aerosol species (black carbon, dust, sea salt, sulfate, and organic carbon) retrieved from the reanalysis datasets. The monthly and seasonal analyses, as well as spatial evaluations, show that AOD levels are most prominent during the spring (MAM) and summer (JJA) seasons, and notably lower in winter (DJF) and autumn (SON). The summer months exhibit the highest AOD levels, particularly in the Sahara and Arabian Deserts, which are the dominant sources of aerosols (Berhane et al. 2024). The findings of MERRA-2, MODIS, and CAMSRA datasets consistently align in terms of seasonal and inter-annual AOD variations, with 2011 and 2012 showing higher AOD values and 2014 and 2020 recording relatively lower values.

The response of the five aerosol species to spatial and temporal influences varies significantly. Dust is the most prevalent aerosol species, contributing the largest proportion to AOD in the region. Black carbon and sea salt aerosols show relatively smaller amounts, owing to the region's

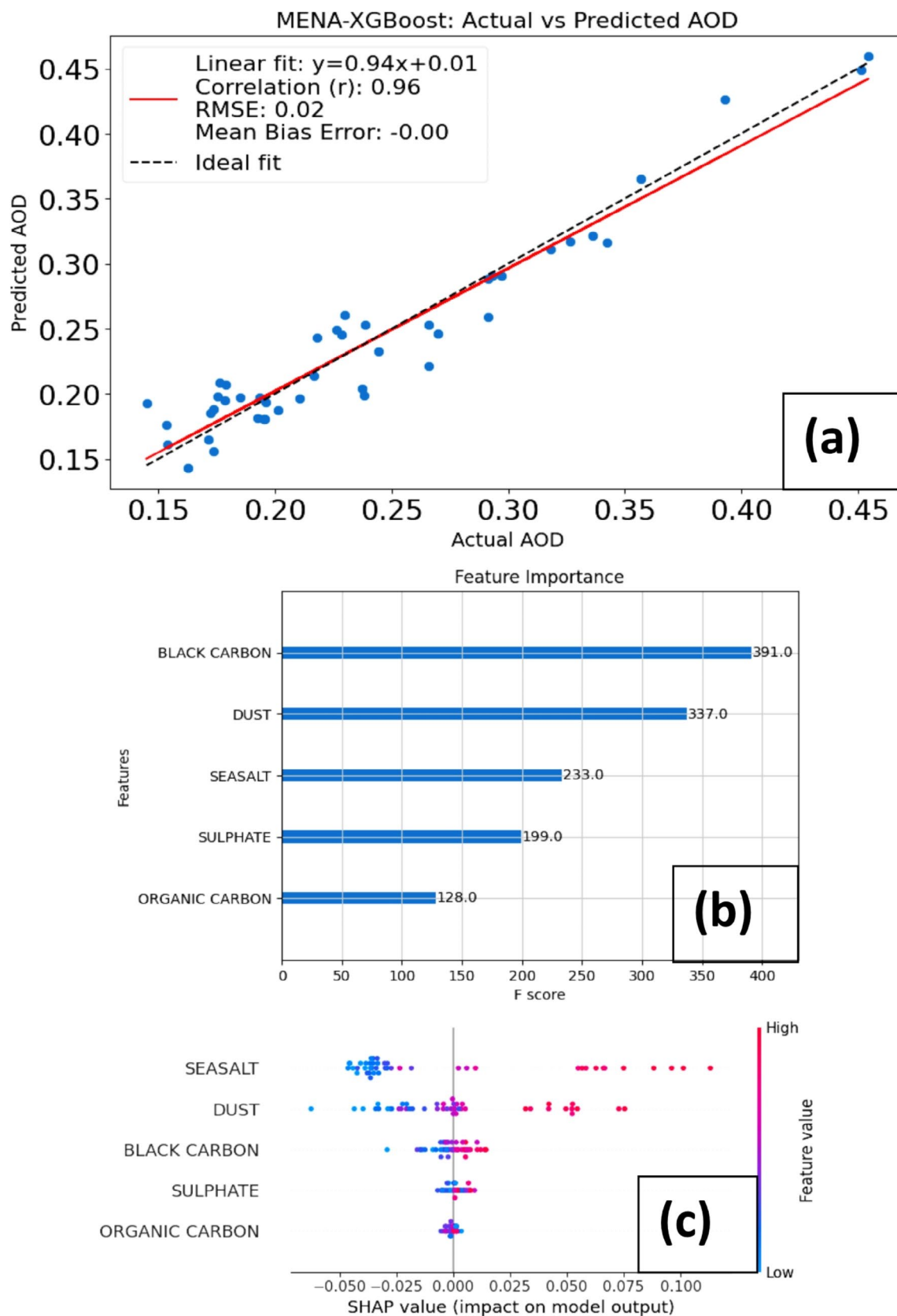


Fig. 13 (a) The Model evaluation of XGBoost performance on AOD, (b) Feature importance (F-score) and (c) SHAP (SHapley Additive exPlanations) value analysis on AOD from each species over the MENA region from 2003 to 2020

geographical location, while organic carbon and sulfate exert a more localized influence. Black carbon is concentrated primarily in Central and West Africa, especially during the winter (DJF) season, attributed to anthropogenic activities such as biomass burning and agricultural practices. Dust, covering nearly 80% of the study area, dominates the MENA region, particularly in the Sahara and Arabian Deserts. Organic carbon is prevalent in Central and West Africa during winter, while sea salt aerosols influence areas along the Red Sea coast. Sulfate aerosols, which are primarily anthropogenic in origin, are found mainly in the Middle East and the Red Sea region, influenced by industrial activities and sea salt particles.

The predictive accuracy of the XGBoost model in estimating AOD over the MENA region from 2003 to 2020 further reinforces these findings. The model shows a strong correlation between predicted and actual AOD values, with minimal error and no significant bias. The most significant contributors to AOD predictions are black carbon and dust, reflecting their key roles in atmospheric opacity and pollution in the region. Dust is especially prominent due to frequent storms and desert conditions, and black carbon associated with industrial emissions, is the dominant factor influencing AOD. Other contributors, such as sea salt, sulfate, and organic carbon, also play important roles, highlighting the complex interplay between natural and anthropogenic aerosols in the region. The SHAP value analysis reveals how each aerosol species contributes to AOD predictions. Dust and sea salt consistently show positive contributions to AOD, aligning with the frequent dust storms and marine aerosol sources in the region. Black carbon displays both positive and negative impacts on AOD, depending on atmospheric conditions, while sulfate and organic carbon demonstrate a more nuanced influence. These findings highlight the importance of both natural and human-made sources in shaping AOD levels across the MENA region.

In conclusion, long-term reanalysis datasets such as MERRA-2 and CAMSRA offer valuable insights into aerosol composition and behavior over the MENA region. Despite the limitations posed by sparse ground-based observations, these datasets complement remote sensing data, providing a comprehensive view of aerosol dynamics. The study emphasizes the significant role of dust and black carbon in driving AOD levels, particularly in desert and industrialized regions. It also stresses the need for continuous monitoring and policy implementation to mitigate air pollution, recognizing that reductions in aerosol concentrations can have broader implications for climate and weather patterns through their effects on rainfall and temperature. As AOD screening techniques continue to improve, the integration of multiple data sources will remain crucial for

accurately assessing and predicting aerosol impacts in the region.

The conclusions of this study align with the United Nation's Sustainable Development Goals (SDGs) that emphasize environmental sustainability, climate action, and public health. SDG 3 of Good Health and Well-being is relevant as the research highlights the health risks associated with aerosol species like black carbon and dust, which contribute to respiratory and cardiovascular diseases. This study supports SDG 13 of Climate Action by emphasizing the need to understand aerosol impact on climate dynamics, aligning with efforts to reduce emissions and mitigate climate change. Additionally, SDG 7 of Affordable and Clean Energy advocates for cleaner energy sources to minimize black carbon emissions. The findings also resonate with SDG 11 of Sustainable Cities and Communities, focusing on improving urban air quality and reducing pollution from industrial activities and transportation over the MENA region. Furthermore, SDG 15 of Life on Land emphasizes the need to manage dust sources to combat desertification, while SDG 6 of Clean Water and Sanitation underscores the importance of reducing atmospheric pollutants that can adversely affect water quality. Overall, this research supports integrated strategies to address air pollution, promote public health, and foster sustainable development across multiple sectors, ultimately contributing to a healthier and more resilient environment for future generations.

Acknowledgements We are thankful for the availability of the MODIS AOD products from Terra and Aqua satellite platforms. The AOD datasets of CAMSRA used in this study were provided through the Copernicus Atmosphere Monitoring Service, funded by the European Union (https://apps.ecmwf.int/data-catalogues/cams-reanalysis/?class=mc&exp_ver=eac4). The MERRA-2 AOD products were provided by GES-DISC (Goddard Earth Science Data and Information Services Center, <https://disc.gsfc.nasa.gov/>, <https://doi.org/10.5067/FH9A0MLJPC7N>). The first author is thankful to the China Scholarship Council and Nanjing University of Information Science and Technology for accommodating a suitable environment to pursue his PhD study. One of the authors, Pelati Althaf, acknowledges the Management of KLEF, India for supporting a research fellowship for the year 2023 and providing the necessary infrastructure facilities to undertake full-time studies in the Doctoral (PhD) program.

Author contributions All authors have read and agreed to the published version of the manuscript. *Samuel Abraham Berhane*: Conceptualization, Formal analysis, Methodology, Data Curation, Visualization, Investigation, Writing-Original draft, Writing-review and editing. *Pelati Althaf*: Data Curation, Methodology, Visualization, Writing-review and editing. *Kanike Raghavendra Kumar*: Methodology, Validations, Funding acquisition, Writing-review and editing. *Lingbing Bu*: Methodology, Supervision, Project Administration, Funding acquisition, Writing-review and editing. *Muxi Yao*: Data Curation, Methodology, Writing-review and editing.

Funding This research was funded by the National Natural Science Foundation of China (Grant No. 42175145) and the Shanghai Aerospace Science and Technology Innovation Foundation (SAST2022-

039). One of the authors, K.R.K. and P.A., thank the Science and Engineering Research Board (SERB), a statutory body under the Department of Science and Technology (DST), New Delhi, India for providing a research grant under the Start-up Research Grant (SRG; File No. SRG/2020/001445) scheme, and awarding the DST-FIST Level-1 (Grant No. SR/FST/PS-1/2018/35) and DST-PURSE (Grant No. SR/PURSE/2023/196) schemes to the Department of Physics, KLEF, India.

Declarations

Conflict of interest The authors declare no conflict of interest.

Ethics Approval The results/data/figures in this manuscript have not been published elsewhere, nor are they under consideration by another publisher.

References

- Aklesso M, Kumar KR, Bu L, Boiyo R (2018) Analysis of spatial-temporal heterogeneity in remotely sensed aerosol properties observed during 2005–2015 over three countries along the Gulf of Guinea Coast in Southern West Africa. *Atmos Environ* 182(February):313–324. <https://doi.org/10.1016/j.atmosenv.2018.03.062>
- Almazroui M (2022) The influence of the Madden–Julian oscillation on the wet season rainfall over Saudi Arabia. *Earth Syst Environ* 7(1):1–14. <https://doi.org/10.1007/s41748-022-00334-w>
- Alam K, Iqbal MJ, Blaschke T, Qureshi S, Khan G (2010) Monitoring spatio-temporal variations in aerosols and aerosol-cloud interactions over Pakistan using MODIS data. *Adv Space Res* 46(9):1162–1176. <https://doi.org/10.1016/j.asr.2010.06.025>
- Ali MA, Assiri M (2019) Analysis of AOD from MODIS-Merged DT–DB products over the Arabian Peninsula. *Earth Syst Environ* 3(3):625–636. <https://doi.org/10.1007/s41748-019-00108-x>
- Ali MA, Bilal M, Wang Y, Qiu Z, Nichol JE, Mhwash A, de Leeuw G, Zhang Y, Shahid S, Almazroui M, Islam MN, Rahman MA, Mondol SK, Tiwari P, Khedher KM (2022) Spatiotemporal changes in aerosols over Bangladesh using 18 years of MODIS and reanalysis data. *J Environ Manage* 315(April):115097. <https://doi.org/10.1016/j.jenvman.2022.115097>
- Altha P, Kumar KR, Kannemadugu HBS (2024) Aerosol Optical Depth over the Andhra Pradesh State in South India from Reanalysis Data: Spatiotemporal Variabilities and Machine Learning Approach. *Earth Syst Environ*. <https://doi.org/10.1007/s41748-024-00465-2>
- Andreae MO, Rosenfeld D (2008) Aerosol-cloud-precipitation interactions. Part 1. The nature and sources of cloud-active aerosols. *Earth Sci Rev* 89(1–2):13–41. <https://doi.org/10.1016/j.earscirev.2008.03.001>
- Assiri ME (2024) Aerosol Types Identification over the Arabian Peninsula Using AERONET Products: Evaluation with Multisource Datasets. *Earth Syst Env* 8(2):483–499. <https://doi.org/10.1007/s41748-024-00389-x>
- Berhane SA, Bu L (2021) Aerosol—Cloud Interaction with Summer Precipitation over Major Cities in Eritrea. *Remote Sens* 13(4):677. <https://doi.org/10.3390/rs13040677>
- Berhane SA, Kumar KR, Bu L (2024) A 13-year space-based climatological evolution of desert dust aerosols in the Middle East and North Africa regions observed by the CALIPSO. *Sci Total Environ* 174793. <https://doi.org/10.1016/j.scitotenv.2024.174793>
- Boiyo R, Kumar KR, Zhao T (2017) Statistical intercomparison and validation of multisensor aerosol optical depth retrievals over three AERONET sites in Kenya, East Africa. *Atmos Res* 197(March):277–288. <https://doi.org/10.1016/j.atmosres.2017.07.012>
- Boiyo R, Kumar KR, Zhao T (2018) Spatial variations and trends in AOD climatology over East Africa during 2002–2016: a comparative study using three satellite data sets. *Int J Climatol* 38:e1221–e1240. <https://doi.org/10.1002/joc.5446>
- Capes G, Johnson B, McFiggans G, Williams PI, Haywood J, Coe H (2008) Aging of biomass burning aerosols over West Africa: aircraft measurements of chemical composition, microphysical properties, and emission ratios. *J Geophys Res Atmos* 113(23):1–13. <https://doi.org/10.1029/2008JD009845>
- Charlson RJ, Schwartz SE, Hales JM, Cess RD, Coakley JA, Hansen JE, Hofmann DJ (1992) Climate forcing by anthropogenic aerosols. *Science* 255(5043):423–430. <https://doi.org/10.1126/science.255.5043.423>
- Choi Y, Chen SH, Huang CC, Earl K, Chen CY, Schwartz CS, Matsui T (2020) Evaluating the Impact of Assimilating Aerosol Optical Depth Observations on Dust forecasts over North Africa and the East Atlantic using different data assimilation methods. *J Adv Model Earth Syst* 12(4):1–30. <https://doi.org/10.1029/2019MS01890>
- Cruz C, Research SP-J (1998) of G., & undefined. (1998). The effect of organic coatings on the cloud condensation nuclei activation of inorganic atmospheric aerosol. *Wiley Online Library*, 103(D11), 111–124. <https://doi.org/10.1029/98JD00979>
- da Silva A, Colarco PR, Darmenov A, Holben BN (2013) Assessing DRAGON Measurements for Evaluation and Assimilation in the GEOS-5 Aerosol Forecasting System. *Assessing DRAGON Measurements for Evaluation and Assimilation in the GEOS-5 Aerosol Forecasting System*, A24C-05
- De Leeuw G, Sogacheva L, Rodriguez E, Kourtidis K, Georgoulias AK, Alexandri G, Amiridis V, Proestakis E, Marinou E, Xue Y, Van Der A, R (2018) Two decades of satellite observations of AOD over mainland China using ATSR-2, AATSR and MODIS/Terra: data set evaluation and large-scale patterns. *Atmos Chem Phys* 18(3):1573–1592. <https://doi.org/10.5194/acp-18-1573-2018>
- Deflorio MJ, Ghan SJ, Singh B, Miller AJ, Cayan DR, Russell LM, Somerville RCJ (2014) Semidirect dynamical and radiative effect of north African dust transport on lower tropospheric clouds over the subtropical north atlantic in CESM 1.0. *J Phys Res* 119(13):8284–8303.
- Factorization M P. (2019) Influence of dust and sea-salt sandwich effect on precipitation chemistry over the western ghats during summer monsoon. 1–13. <https://doi.org/10.1038/s41598-019-55245-0>
- Flemming J, Benedetti A, Inness A, Engelen J, Jones R, Huijnen L, Remy V, Parrington S, Suttie M, Bozzo M, Peuch A, Akritidis VH, D., Katragkou E (2017) The CAMS interim reanalysis of Carbon Monoxide, ozone and aerosol for 2003–2015. *Atmos Chem Phys* 17(3):1945–1983. <https://doi.org/10.5194/acp-17-1945-2017>
- Francis D, Chaboureau J, Nelli N, Cuesta J, Alshamsi N, Temimi M, Pauluis O, Xue L (2020) Summertime dust storms over the Arabian Peninsula and impacts on radiation, circulation, cloud development and rain. *Atmos Res* 250:105364. <https://doi.org/10.1016/j.atmosres.2020.105364>
- Ganguly D, Jayaraman A, Gadhavi H (2006) Physical and optical properties of aerosols over an urban location in western India: Seasonal variabilities. *J Geophys Res Atmos* 111(24):1–21. <https://doi.org/10.1029/2006JD007392>
- Gelaro R, McCarty W, Suárez MJ, Todling R, Molod A, Takacs L, Randles CA, Darmenov A, Bosilovich MG, Reichle R, Wargan K, Coy L, Cullather R, Draper C, Akella S, Buchard V, Conaty A, da Silva AM, Gu W, Zhao B (2017) The modern-era retrospective analysis for research and applications, version 2 (MERRA-2). *J Clim* 30(14):5419–5454. <https://doi.org/10.1175/JCLI-D-16-0758.1>

- Gong SL, Barrie LA, Blanchet JP (1997) Modeling sea-salt aerosols in the atmosphere 1. Model development. *J Geophys Res Atmos* 102(3):3805–3818. <https://doi.org/10.1029/96jd02953>
- Goudie AS (2014) Desert dust and human health disorders. *Environ Int* 63:101–113. <https://doi.org/10.1016/j.envint.2013.10.011>
- Gui K, Che H, Zeng Z, Wang Y, Zhai S, Wang Z, Luo M, Zhang L, Liao T, Zhao H, Li L, Zheng Y, Zhang X (2020) Construction of a virtual PM_{2.5} observation network in China based on high-density surface meteorological observations using the extreme gradient boosting model. *Environ Int* 141:105801. <https://doi.org/10.1016/j.envint.2020.105801>
- Guleria RP, Kuniyal JC, Dhyani PP, Joshi R, Sharma NL (2014) Impact of aerosol on surface reaching solar irradiance over Mohal in the northwestern Himalaya, India. *J Atmos Solar Terr Phys* 108:41–49. <https://doi.org/10.1016/j.jastp.2013.12.002>
- Gunthe SS, Liu P, Panda U, Raj SS, Sharma A, Derbyshire E, Reyes-Villegas E, Allan J, Chen Y, Wang X, Song S, Pöhlker ML, Shi L, Wang Y, Kommula SM, Liu T, Ravikrishna R, McFiggans G, Mickley LJ, Coe H (2021) Enhanced aerosol particle growth sustained by high continental chlorine emission in India. *Nat Geosci* 14(2):77–84. <https://doi.org/10.1038/s41561-020-00677-x>
- Gupta P, Remer LA, Patadia F, Levy RC, Christopher SA (2020) *High-Resolution Gridded Level 3 Aerosol Optical Depth Data from MODIS*
- Hamzeh NH, Karami S, Kaskaoutis DG, Tegen I, Moradi M, Opp C (2021) Atmospheric dynamics and numerical simulations of six frontal dust storms in the Middle East region. *Atmos* 12(1):125. <https://doi.org/10.3390/atmos12010125>
- He Q, Li C, Mao J, Lau AKH, Chu DA (2008) Analysis of aerosol vertical distribution and variability in Hong Kong. *J Geophys Res Atmos* 113(14):1–13. <https://doi.org/10.1029/2008JD009778>
- Hu K, Kumar KR, Kang N, Boiyo R, Wu J (2018) Spatiotemporal characteristics of aerosols and their trends over mainland China with the recent Collection 6 MODIS and OMI satellite datasets. *Environ Sci Pollut Res* 25(7):6909–6927. <https://doi.org/10.1007/s11356-017-0715-6>
- Huang J, Wang T, Wang W, Li Z, Yan H (2014) Climate effects of dust aerosols over east Asian arid and semiarid regions. *Nature* 175(4449):238. <https://doi.org/10.1038/175238c0>
- Huang X, Ding A, Liu L, Liu Q, Ding K, Niu X, Nie W, Xu Z, Chi X, Wang M, Sun J, Guo W, Fu C (2016) Effects of aerosol-radiation interaction on precipitation during biomass-burning season in East China. *Atmos Chem Phys* 16(15):10063–10082. <https://doi.org/10.5194/acp-16-10063-2016>
- Huang G, Chen Y, Li Z, Liu Q, Wang Y, He Q, Liu T, Liu X, Zhang Y, Gao J, Yao Y (2020) Validation and accuracy analysis of the Collection 6.1 MODIS aerosol optical depth over the Westernmost City in China based on the Sun-Sky Radiometer observations from SONET. *Earth Space Sci* 7(3). <https://doi.org/10.1029/2019EA001041>
- Huang F, Ma W, Wang S, Feng C, Kong X, Liu H (2023) *Analysis and Validation of the Aerosol Optical Depth of*. 1–12
- Huneeus N, Schulz M, Balkanski Y, Griesfeller J, Prospero J, Kinne S, Bauer S, Boucher O, Chin M, Dentener F, Diehl T, Easter R, Fillmore D, Ghan S, Ginoux P, Grini A, Horowitz L, Koch D, Krol MC, Zender CS (2011) Global dust model intercomparison in AeroCom phase i. *Atmos Chem Phys* 11(15):7781–7816. <https://doi.org/10.5194/acp-11-7781-2011>
- Hsu NC, Gautam R, Sayer AM, Bettenhausen C, Li C, Jeong MJ, Tsay S, Holben BN (2012) Global and regional trends of aerosol optical depth over land and ocean using SeaWiFS measurements from 1997 to 2010. *Atmos Chem Phys* 12(17):8037–8053. <https://doi.org/10.5194/acp-12-8037-2012>
- Inness A, Ades M, Agustí-Panareda A, Barr J, Benedictow A, Blechschmidt AM, Jose Dominguez J, Engelen R, Eskes H, Flemming J, Huijnen V, Jones L, Kipling Z, Massart S, Parrington M, Peuch VH, Razinger M, Remy S, Schulz M, Suttie M (2019) The CAMS reanalysis of atmospheric composition. *Atmos Chem Phys* 19(6):3515–3556. <https://doi.org/10.5194/acp-19-3515-2019>
- IPCC, 2021. Climate Change 2021: The Physical Science Basis. Contribution of Working Group I to the Sixth 49(4):44–45. <https://search.informit.org/doi/10.3316/informit.315096509383738>
- Islam MN, Ali MA, Islam MM (2019) Spatiotemporal investigations of aerosol optical properties over Bangladesh for the period 2002–2016. *Earth Syst Environ* 3(3):563–573. <https://doi.org/10.1007/s41748-019-00120-1>
- Karami K, Tilmes S, Muri H, Mousavi SV (2020) Storm track changes in the Middle East and North Africa under Stratospheric Aerosol Geoengineering. *Geophys Res Lett* 47(14). <https://doi.org/10.1029/2020GL086954>
- Karami S, Kaskaoutis DG, Pytharoulis I, Sotiropoulou RP, Tagaris E (2024) Dust transport from North Africa to the Middle East: synoptic patterns and numerical forecast. *Atmosphere* 15(5):531. <https://doi.org/10.3390/atmos15050531>
- Khamala GW, Makokha JW, Boiyo R, Kumar KR (2022) Spatiotemporal analysis of absorbing aerosols and radiative forcing over environmentally distinct stations in East Africa during 2001–2018. *Sci Total Environ* 864:161041. <https://doi.org/10.1016/j.scitotenv.2022.161041>
- Kinne S, Lohmann U, Feichter J, Schulz M, Timmreck C, Ghan S, Easter R, Chin M, Ginoux P, Takemura T, Tegen I, Koch D, Herzog M, Penner J, Pitari G, Hoibon B, Eck T, Smirnov A, Dubovik O, Kaufman Y (2003) Monthly averages of aerosol properties: a global comparison among models, satellite data, and AERONET ground data. *J Geophys Res Atmos* 108(20). <https://doi.org/10.1029/2001JD001253>
- Klingmüller K, Pozzer A, Metzger S, Stenchikov GL, Lelieveld J (2016) Aerosol optical depth trend over the Middle East. *Atmos Chem Phys* 16(8):5063–5073. <https://doi.org/10.5194/acp-16-5063-2016>
- Knippertz P, Todd MC (2012) Mineral dust aerosols over the Sahara: Meteorological controls on emission and transport and implications for modeling. *Rev Geophys* 50(1). <https://doi.org/10.1029/2011RG000362>
- Kumar KR, Sivakumar V, Reddy RR, Gopal KR, Adesina AJ (2013) Inferring wavelength dependence of AOD and Ångström exponent over a sub-tropical station in South Africa using AERONET data: influence of meteorology, long-range transport and curvature effect. *Sci Total Environ* 461–462:397–408. <https://doi.org/10.1016/j.scitotenv.2013.04.095>
- Kumar KR, Attada R, Dasari HP, Vellore RK, Langodan S, Abualnaja YO, Hoteit I (2018) Aerosol Optical Depth variability over the Arabian Peninsula as inferred from satellite measurements. *Atmos Environ* 187:346–357. <https://doi.org/10.1016/j.atmosenv.2018.06.011>
- Kumar KR, Boiyo R, Madina A, Kang N (2018) A 13-year climatological study on the variations of aerosol and cloud properties over Kazakhstan from remotely sensed satellite observations. *J Atmos Solar Terr Phys* 179(March):55–68. <https://doi.org/10.1016/j.jastp.2018.06.014>
- Kunchala RK, Attada R, Karumuri RK, Seelanki V, Singh BB, Ashok K, Hoteit I (2024) Climatology, trends, and future projections of aerosol optical depth over the Middle East and North Africa region in CMIP6 models. *Front Clim* 6. <https://doi.org/10.3389/clim.2024.1384202>
- Kuttippurath J, Raj S (2021) Two decades of aerosol observations by AATSR, MISR, MODIS and MERRA-2 over India and Indian Ocean. *Remote Sens Environ* 257(March):112363. <https://doi.org/10.1016/j.rse.2021.112363>
- Laruelle GG, Lauerwald R, Pfeil B, Regnier P (2014) Global biogeochemical cycles. *Glob Biogeochem Cycles* 1199–1214. <https://doi.org/10.1002/2013GB004802>. Received

- Levy RC, Remer LA, Kleidman RG, Matto S, Ichoku C, Kahn R, Eck TF (2010) Global evaluation of the Collection 5 MODIS dark-target aerosol products over land. *Atmos Chem Phys* 10(21):10399–10420. <https://doi.org/10.5194/acp-10-10399-2010>
- Li J, Carlson BE, Yung YL, Lv D, Hansen J, Penner JE, Liao H, Ramaswamy V, Kahn RA, Zhang P, Dubovik O, Ding A., Lacis AA, Zhang L, Dong Y (2021) Scattering and absorbing aerosols in the climate system. *Nat Rev Earth Environ* 3(6):363–379. <https://doi.org/10.1038/s43017-022-00296-7>
- Li Z, Lau WKM, Ramanathan V, Wu G, Ding Y, Manoj MG, Liu J, Qian Y, Li J, Zhou T, Fan J, Rosenfeld D, Ming Y, Wang Y, Huang J, Wang B, Xu X, Lee SS, Crabb M, Brasseur GP (2016) Aerosol and monsoon climate interactions over Asia. In: *Reviews of Geophysics*. <https://doi.org/10.1002/2015RG000500>
- Liu X, Penner JE, Herzog M (2005) *Global modeling of aerosol dynamics: Model description, evaluation, and interactions between sulfate and nonsulfate aerosols.* 110, 1–37. <https://doi.org/10.1029/2004JD005674>
- Liu H, Yan R, Yang J (2021) Credibility and statistical characteristics of CAMSRA and MERRA-2 AOD reanalysis products over the Sichuan Basin during 2003–2018. *Atmos Environ* 244(June 2020):117980. <https://doi.org/10.1016/j.atmosenv.2020.117980>
- Mahowald N, Albani S, Kok JF, Engelstaeder S, Scanza R, Ward DS, Flanner MG (2014) The size distribution of desert dust aerosols and its impact on the Earth system. *Aeolian Res* 15:53–71. <https://doi.org/10.1016/j.aeolia.2013.09.002>
- Masoud AA (2023) Spatio-temporal patterns and trends of the air pollution integrating MERRA-2 and in situ air quality data over Egypt (2013–2021). *Air Qual Atmos Health* 2050(0123456789). <https://doi.org/10.1007/s11869-023-01357-6>
- McCarty W, Coy L, Gelaro R, Huang A, Merkova D, Smith EB, Sienkiewicz M, Wargan K (2016) *MERRA-2 Input Observations: Summary and Assessment. Technical Report Series on Global Modeling and Data Assimilation* 46. 46(October), 51
- Menut L, Tuccella P, Flamant C, Deroubaix A, Gaetani M (2019) The role of aerosol-radiation-cloud interactions in linking anthropogenic pollution over Southern West Africa and dust emission over the Sahara. *Atmos Chem Phys* 19(23):14657–14676. <https://doi.org/10.5194/acp-19-14657-2019>
- Migoń P, Duszyński F, Goudie A (2017) Rock cities and ruiform relief: forms – processes – terminology. *Earth Sci Rev* 171(May):78–104. <https://doi.org/10.1016/j.earscirev.2017.05.012>
- Nielsen JE, Pawson S, Molod A, Auer B, da Silva AM, Douglass AR, Duncan B, Liang Q, Manyin M, Oman LD, Putman W, Strahan SE, Wargan K (2017) Chemical mechanisms and their applications in the Goddard Earth Observing System (GEOS) Earth System Model. *J Adv Model Earth Syst* 9(8):3019–3044. <https://doi.org/10.1002/2017MS001011>
- Notaro M, Yu Y, Kalashnikova OV (2015) Regime shift in Arabian dust activity, triggered by persistent Fertile Crescent drought. *J Geophys Res Atmos* 120(19). <https://doi.org/10.1002/2015jd023855>
- Ou Y, Li Z, Chen C, Zhang Y, Li K, Shi Z, Dong J, Xu H, Peng Z, Xie Y, Luo J (2022) Evaluation of MERRA-2 Aerosol Optical and Component properties over China using SONET and PARASOL/GRASP data. *Remote Sens* 14(4). <https://doi.org/10.3390/rs14-40821>
- Parajuli S, Stenckov GG, Ukhov A, Shevchenko I, Dubovik O, Lopatin A (2020) Aerosol vertical distribution and interactions with land/sea breezes over the eastern coast of the Red Sea from lidar data and high-resolution WRF-Chem simulations. *Atmos Chem Phys* 20(24):16089–16116. <https://doi.org/10.5194/acp-20-16089-2020>
- Peshev Z, Chaikovsky A, Evgenieva T, Pescherenkov V, Vulкова L, Deleva A, Dreischuh T (2023) Combined characterization of Airborne Saharan Dust above Sofia, Bulgaria, during blocking-pattern conditioned Dust Episode in February 2021. *Remote Sens* 15(15). <https://doi.org/10.3390/rs15153833>
- Prijith SS, Aloysius M, Mohan M (2014) Relationship between wind speed and sea salt aerosol production: a new approach. *J Atmos Solar Terr Phys* 108:34–40. <https://doi.org/10.1016/j.jastp.2013.12.009>
- Prospero JM (1999) Long-range transport of mineral dust in the global atmosphere: impact of African dust on the environment of the southeastern United States. *Proc Natl Acad Sci USA* 96(7):3396–3403. <https://doi.org/10.1073/pnas.96.7.3396>
- Prospero JM, Delany AC, Delany AC, Carlson TN (2021) The discovery of African dust transport to the western hemisphere and the Saharan air layer: a history. *Bull Am Meteorol Soc* 102(6):E1239–E1260. <https://doi.org/10.1175/BAMS-D-19-0309.1>
- Raghavendra Kumar K, Narasimulu K, Balakrishnaiah G, Suresh Kumar Reddy B, Rama Gopal K, Reddy RR, Moorthy KK, Babu S, S (2009) Size segregated mass concentration and size distribution of near surface aerosols over a tropical Indian semi-arid station, Anantapur: impact of long range transport. *Sci Total Environ* 407(21):5589–5604. <https://doi.org/10.1016/j.scitotenv.2009.06.039>
- Ramanathan V, Crutzen PJ, Kiehl JT, Rosenfeld D (2001) Aerosols, climate, and the hydrological cycle. *Science* 294(5549):2119–2124. <https://doi.org/10.1126/science.1064034>
- Ramachandran S, Srivastava R, Kedia S, Rajesh TA (2012) Contribution of natural and anthropogenic aerosols to optical properties and radiative effects over an urban location. *Environ Res Lett* 7(3). <https://doi.org/10.1088/1748-9326/7/3/034028>
- Remer LA, Kaufman YJ, Tanré D, Matto S, Chu DA, Martins JV, Li R, Ichoku C, Levy RC, Kleidman RG, Eck TF, Vermote E, Holben BN (2005) The MODIS Aerosol Algorithm, products, and validation. *J Atmos Sci* 62(4):947–973. <https://doi.org/10.1175/jas3385.1>
- Ridley DA, Heald CL, Prospero JM (2014) What controls the recent changes in African mineral dust aerosol across the Atlantic? *Atmos Chem Phys* 14(11):5735–5747. <https://doi.org/10.5194/acp-14-5735-2014>
- Rocha-Lima A, Colarco PR, Darmenov AS, Nowotnick EP, Da Silva AM, Oman LD (2024) Investigation of observed dust trends over the Middle East region in NASA Goddard Earth Observing System (GEOS) model simulations. *Atmos Chem Phys* 24(4):2443–2464. <https://doi.org/10.5194/acp-24-2443-2024>
- Rosenfeld D, Lohmann U, Raga GB, O'Dowd CD, Kulmala M, Fuzzi S, Reissell A, Andreae MO (2008) Flood or drought: How do aerosols affect precipitation? In: *Science*. <https://doi.org/10.1126/science.1160606>
- Rosenfeld D, Andreae MO, Asmi A, Chin M, De Leeuw G, Donovan DP, Kahn R, Kinne S, Kivekäs N, Kulmala M, Lau W, Schmidt KS, Suni T, Wagner T, Wild M, Quaas J (2014) Global observations of aerosol-cloud-precipitation-climate interactions. *Rev Geophys*. <https://doi.org/10.1002/2013RG000441>
- Ryder CL, Highwood EJ, Rosenberg PD, Trembath J, Brooke JK, Bart M, Dean A, Crosier J, Dorsey J, Brindley H, Banks J, Marsham JH, McQuaid JB, Sodemann H, Washington R (2013) Optical properties of Saharan dust aerosol and contribution from the coarse mode as measured during the Fennec 2011 aircraft campaign. *Atmos Chem Phys* 13(1):303–325. <https://doi.org/10.5194/acp-13-303-2013>
- Sanatan B, Vinoj V, David LM, Sen IS (2024) Long-range transport of aerosols and regional sources using MODIS and NASA MERRA reanalysis over South Asia. *Earth Syst Environ*. <https://doi.org/10.1007/s41748-024-00478-x>
- Sangura MT, Althaf P, Makokha JW, Boiyo R, Kumar KR (2024) Estimation and Model Performance of Aerosol Radiative Forcing from Radiative Transfer Models using the AERONET Data over

- Kenya, East Africa. *Adv Space Res* <https://doi.org/10.1016/j.asr.2024.09.061>
- Saturno J, Holanda BA, Pöhlker C, Ditas F, Wang Q, Moran-Zuloaga D, Brito J, Carbone S, Cheng Y, Chi X, Ditas J, Hoffmann T, De Angelis H, Könemann I, Lavrič T, Ma JV, Ming N, Paulsen J, Pöhlker H, Andreae ML, M. O (2018) Black and brown carbon over central Amazonia: long-term aerosol measurements at the ATTO site. *Atmos Chem Phys* 18(17):12817–12843. <https://doi.org/10.5194/acp-18-12817-2018>
- Shaheen A, Wu R, Aldabash M (2020) Long-term AOD trend assessment over the Eastern Mediterranean region: a comparative study including a new merged aerosol product. *Atmos Environ* 238:117736. <https://doi.org/10.1016/j.atmosenv.2020.117736>
- Shaheen A, Wu R, Yousefi R, Wang F, Ge Q, Kaskaoutis DG, Wang J, Alpert P, Munawar I (2022) Spatio-temporal changes of spring-summer dust AOD over the Eastern Mediterranean and the Middle East: reversal of dust trends and associated meteorological effects. *Atmos Res* 281:106509. <https://doi.org/10.1016/j.atmosres.2022.106509>
- Shaheen A, Wang F, Yousefi R, Ge Q, Wu R, Liu M, Kaskaoutis DG, Bilal M (2024) Space-time evaluation of atmospheric black carbon in Chinese urban environment: influence of land use and air pollution policies. *Earth Syst Environ*. <https://doi.org/10.1007/s41748-024-00380-6>
- Shahid MZ, Chishtie F, Bilal M, Shahid I (2021) Wrf-chem simulation for modeling seasonal variations and distributions of aerosol pollutants over the Middle East. *Remote Sens* 13(11):1–17. <https://doi.org/10.3390/rs13112112>
- Sogacheva L, Kolmonen P, Virtanen TH, Rodriguez E, Saponaro G, De Leeuw G (2017) Post-processing to remove residual clouds from aerosol optical depth retrieved using the Advanced along Track scanning Radiometer. *Atmos Meas Tech* 10(2):491–505. <https://doi.org/10.5194/amt-10-491-2017>
- Textor C, Schulz M, Guibert S, Kinne S, Balkanski Y, Bauer S, Berntsen T, Berglen T, Boucher O, Chin M, Dentener F, Diehl T, Easter R, Feichter H, Fillmore D, Ghan S, Ginoux P, Gong S, Grini A, Tie X (2006) Analysis and quantification of the diversities of aerosol life cycles within AeroCom. *Atmos Chem Phys* 6(7):1777–1813. <https://doi.org/10.5194/acp-6-1777-2006>
- Tindan JZ, Jin Q, Pu B (2023) Understanding day-night differences in dust aerosols over the dust belt of North Africa, the Middle East, and Asia. *Atmos Chem Phys* 23(9):5435–5466. <https://doi.org/10.5194/acp-23-5435-2023>
- Vandenbussche S, De Mazière M (2017) African mineral dust sources: a combined analysis based on 3D dust aerosols distributions, winds and surface parameters. *Atmospheric Chem Phys Discuss* 1–37. <https://doi.org/10.5194/acp-2017-809>
- Wang W, Evan AT, Flamant C, Lavaysse C (2015) On the decadal scale correlation between African dust and Sahel rainfall: the role of Saharan heat low-forced winds. *Sci Adv* 1(9):2010–2015. <https://doi.org/10.1126/sciadv.1500646>
- Weir B, Crisp D, O'Dell CW, Basu S, Chatterjee A, Kolassa J, Oda T, Pawson S, Poulter B, Zhang Z, Ciais P, Davis SJ, Liu Z, Ott LE (2021) Regional impacts of COVID-19 on carbon dioxide detected worldwide from space. *Sci Adv* 7(45):1–10. <https://doi.org/10.1126/sciadv.abf9415>
- Xu X, Wu H, Yang X, Xie L (2020) Distribution and transport characteristics of dust aerosol over Tibetan Plateau and Taklimakan Desert in China using MERRA-2 and CALIPSO data. *Atmos Environ* 237(March):117670. <https://doi.org/10.1016/j.atmosenv.2020.117670>
- Yoon YJ, Ceburnis D, Cavalli F, Jourdan O, Putaud JP, Facchini MC, Decesari S, Fuzzi S, Sellegrí K, Jennings SG, O'Dowd CD (2007) Seasonal characteristics of the physicochemical properties of North Atlantic Marine atmospheric aerosols. *J Geophys Res Atmos* 112(4):1–14. <https://doi.org/10.1029/2005JD007044>
- Yousefi R, Wang F, Ge Q, Shaheen A, Kaskaoutis DG (2023) Analysis of the Winter AOD trends over Iran from 2000 to 2020 and Associated Meteorological effects. *Remote Sens* 15(4):905. <https://doi.org/10.3390/rs15040905>
- Yu X, Lü R, Kumar KR, Ma J, Zhang Q, Jiang Y, Kang N, Yang S, Wang J, Li M (2016) Dust aerosol properties and radiative forcing observed in spring during 2001–2014 over urban Beijing, China. *Environ Sci Pollut Res* 23(15):15432–15442. <https://doi.org/10.1007/s11356-016-6727-9>
- Zhang X, Lu N, Jiang H, Yao L (2020) Evaluation of Reanalysis Surface Incident Solar Radiation Data in China. *Sci Rep* 10(1):1–20. <https://doi.org/10.1038/s41598-020-60460-1>

Publisher's Note Springer Nature remains neutral with regard to jurisdictional claims in published maps and institutional affiliations.

Springer Nature or its licensor (e.g. a society or other partner) holds exclusive rights to this article under a publishing agreement with the author(s) or other rightsholder(s); author self-archiving of the accepted manuscript version of this article is solely governed by the terms of such publishing agreement and applicable law.